The RAGazine

Volume 3 Issue 1 August 2015

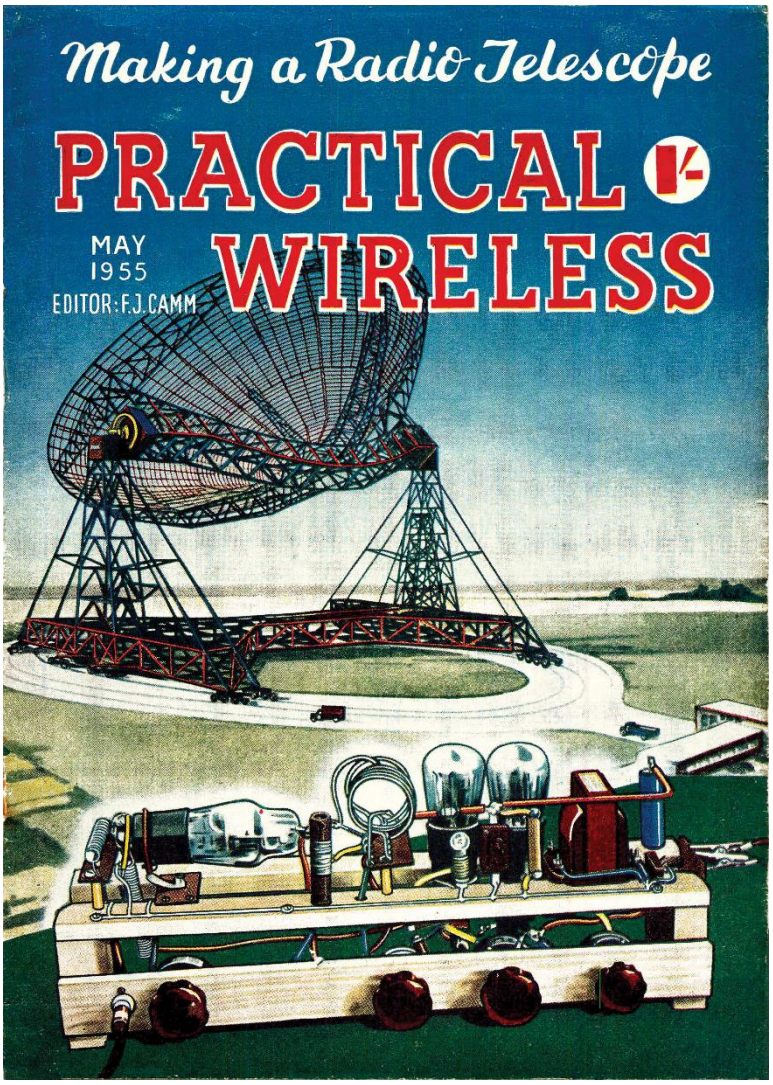

Retro Radio Telescope design from the 1950's inside

August 2015

BAA, Burlington House,
Picadilly,
London
(+44)207 734 4145

The RAGazine

British Astronomical Association
Radio Astronomy Group

Reg Charity 210769

BAA RAG Coordinator **Paul Hyde** g4csd@yahoo.co.uk
Ragazine Editor **Jeff Lashley** jeffl@spacecentre.co.uk
VLF reports **John Cook** jacook@jacook.plus.com
Web : http://www.britastro.org/radio

Notes for content submission

Content should be emailed to the Ragazine editor a minimum of fourteen days before the next publication date. Content submitted after that may not appear the next issue, but will be held for a later issue.

Observational reports are very welcome on topics where radio techniques are applied to observe astronomical objects, or geophysical events. Articles are welcome on topics of radio astronomy observational techniques, radio hardware and related technology, scientific programming, events, data processing, educational out-reach, book reviews, radio astronomy history etc.

The preferred format for submissions is Microsoft Word (.doc or .docx format). However I know that not everyone has access to Microsoft Office, note that the free office suite LibreOffice is available for Windows, Linux and Mac OS. Note that LibreOffice can save documents in Microsoft Word .docx format. If neither of these applications are available then plain text (.txt) is fine.

Images can be supplied embedded in the document or as separate files. Please include the author credits you require to be included in the article, and indicate whether you want your email address to be shown in the publication.

The BAA is not responsible for the opinions expressed by RAGazine contributors, and such published material does not necessarily express the views of BAA Council or RAG officers. Material without attribution is generally contributed by the editor.

2015 Publication dates and submission deadlines

Release Date	Submission deadline
9th November 2015	26th October 2015
14th March 2016	29th April 2016
8th August 2016	25th July 2016

RAG Coordinator report

By Paul Hyde

Welcome to the latest edition of RAGazine and, once again, my thanks to Jeff Lashley for pulling this together and to all those providing the very essential content.

It's been a busy period since the last edition with the BAA Exhibition meeting in Cardiff, where we had a steady stream of people visiting the RAG stand. There have also been talks at West Kent, Harrow and Basing stoke radio clubs and Wycombe, Heart of England and York astronomy societies.

A particularly interesting event was the BAA Meteor Section meeting in Birmingham where there was evident interest in what Meteor Scatter has to offer. I'm pleased to announce that RAG will be holding a Workshop event on this subject at the Northampton Natural History Society on Saturday 31st October. The day will be aimed at both those wanting to get started in this field and existing observers who would like to develop their observing activities. Our keynote speaker will be Jean-Louis Rault, Director of the Radio Section of the International Meteor Organisation, who will be talking about the opportunities for serious observing work. Meteor Scatter is an ideal target for amateur involvement because the entry barriers are relatively low whilst meteors exhibit very dynamic behaviour where radio observations can supplement optical work.

I have offers of supporting presentations from Richard Fleet, Chris Jackson, Jeff Lashley, Jim and Gerry Lowe, and Victoria Penrice but I would love to hear from anyone else who could offer either a presentation or a display or poster on the work that they or their local society has been involved in.

Other upcoming events are Karen Holland's talk at the BAA Back to Basics meeting at St Asaph on 10th October and I will be providing a talk to Birmingham Astronomical Society on 27th October. See the relevant websites for up-to-date information on these meetings.

My thanks to David Morgan for sending me a copy of the 1955 Practical Wireless article on building a radio telescope and which has been reprinted here with the kind permission of PW Publishing Ltd. It makes fascinating reading, especially when you get to the 25 r.p.s. rotors in the receiver!

Please think about whether you can provide material for future editions of RAGazine. We are particularly looking for reports on what people are doing, either individually or as part of a local society or club, to encourage others who are thinking of having a go. But any material related to amateur radio astronomy and geophysics will be welcome.

Solar Activity Second Quarter 2015

By John Cook

Fig 1 shows activity levels since 2005. Sunspot numbers are courtesy of the BAA Solar Section. SID numbers since the last report are as follows:-

April = 48 (including 9 M-class)

May = 49 (including 5 M-class and 1 X-class)

June = 65 (including 8 M-class.)

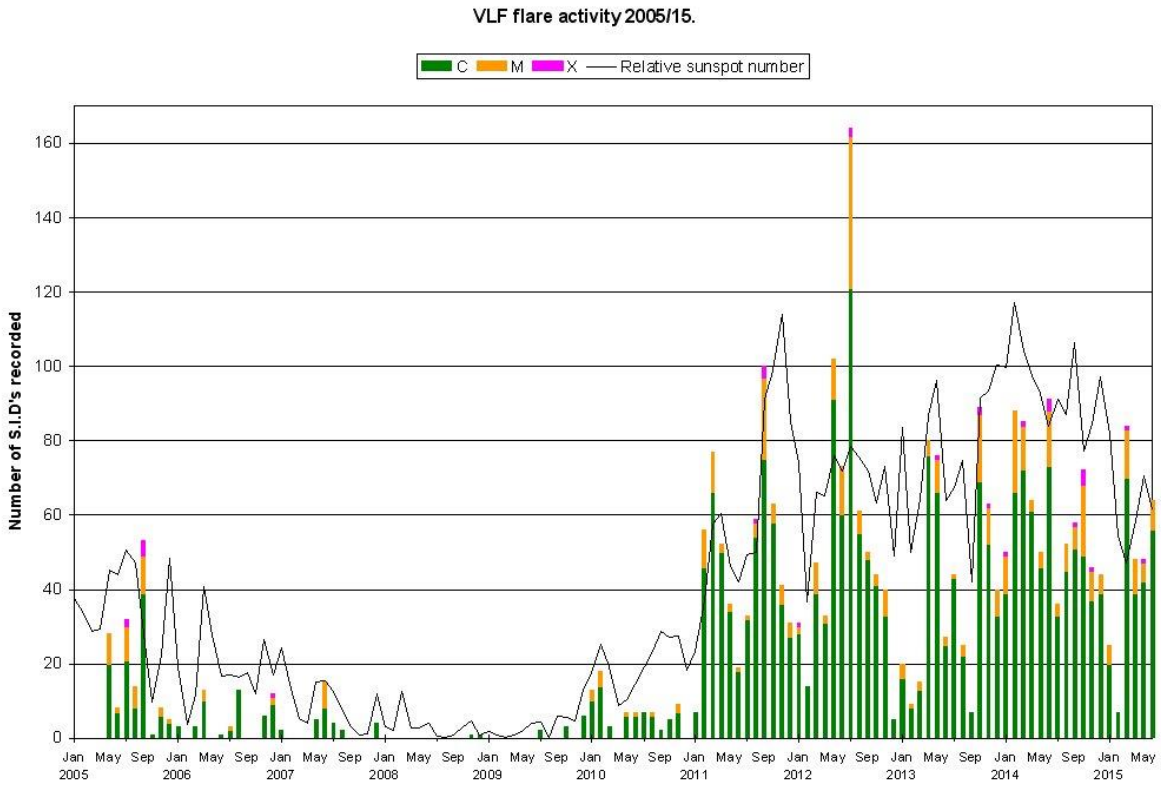

Fig 1: Activity chart.

With 10 years of data recorded in Fig 1, we now have nearly a complete solar cycle. I have tried to keep a consistent approach in analysing the monthly reports, although the group membership has changed over time. I use the Space Weather Prediction Centre (SWPC) bulletins to assign SIDs to solar flares, and the GOES X-ray data files to identify the many multiple-peaked flares that give rise to multiple SIDs. The relative sunspot numbers from the BAA Solar section are an average of about 40 observers with worldwide coverage. Both sets of figures are to the same scale on the vertical axis of fig 1. There is an unfortunate annual distortion to the SID numbers, in that we have a much longer daytime observing period during

the summer compared to winter. SID counts in winter are therefore always lower than in summer given the same level of solar activity.

A very slow M1.1 flare on April 12th provides a good example of how difficult it can sometimes be to measure the start, peak and end times of a SID. See Fig 2. There is a short break in the GOES15 X-ray data (black trace) just before the flare starts, but it reaches a maximum value at 09:42UT before a slow decay lasting until 14:30. My 23.4 kHz recording (red trace) shows a sudden drop in signal level at 09:20. The rate of signal level drop slows down at 09:34 (point A) before reaching its minimum at 10:08 (point B). Neither of these points is the true X-ray minimum, although point A has traditionally been used as the 'peak' time of the SID. Measurements at 22.1 kHz (blue trace) are completely different. It appears that the sky-wave/ground-wave interference pattern is just changing from cancelling to adding at point A as the X-ray flux begins to flatten off. The phase change remains very small until point B, when the drop in X-ray flux allows the phase to return to cancelling. The result is a SID half way between the 'sharks fin' shape and the 'spike and wave' shape.

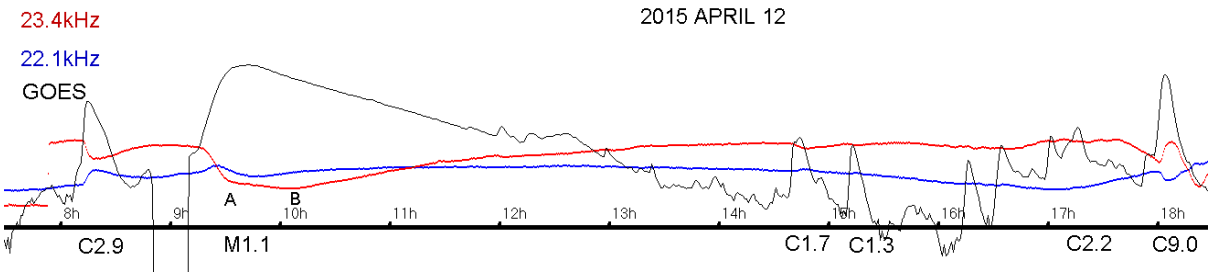

Fig 2: April 12th. John Cook, Wolverhampton.

Fig 3 shows a much shorter M1.1 flare recorded by Roberto Battaiola on April 22nd at 20.3 kHz. This one has produced a more conventional SID, more easily measured along with some smaller C-class flares.

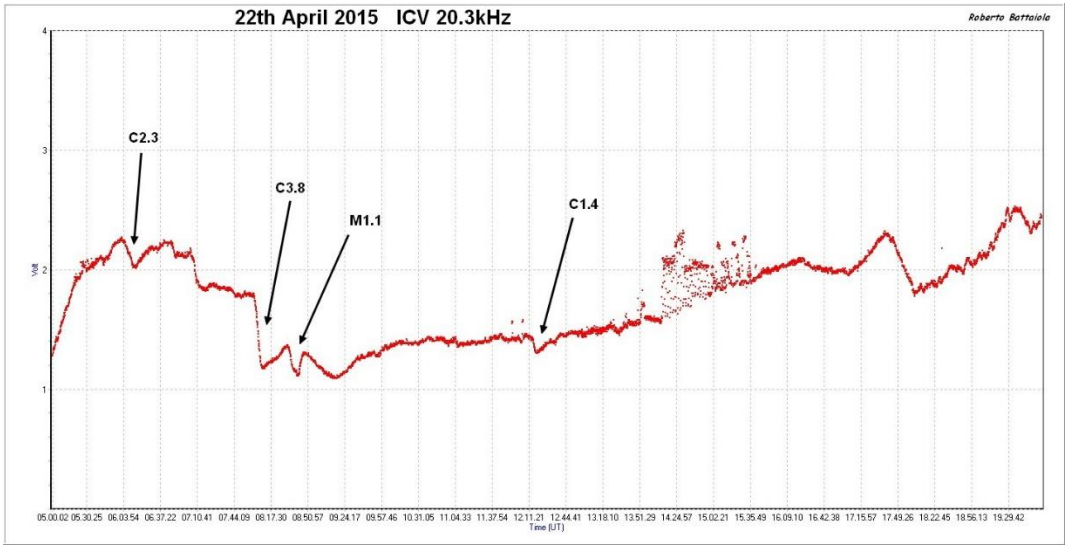

Fig 3: April 22nd. Roberto Battaiola, Milan.

An SFE was produced by a very fast M1.4 flare on April 8th at 14:45UT. Active region AR12320 was responsible for the flare, and may well be making a repeat appearance after crossing the far side of the Sun. The two SFEs from March mentioned in the May Ragazine (Vol. 2 Issue 4) may well be from the same active region during its previous rotation. Both were at similar heliocentric positions, 15 degrees south and close to 200 degrees longitude.

There was a small increase in activity in May, including a strong X2.7 flare on the 5th. Unfortunately it occurred rather late in the evening, around 22:15UT, and so was only seen as a SID on the 24 kHz trans-Atlantic path. This was also the busiest day of the month, as shown in Fig 4 from Mark Edwards. In contrast to the April 12th SID, these are all neat 'sharks-fins', the two signals producing opposite polarity responses. Yellow is 19.6 kHz, brown is 20.9 kHz.

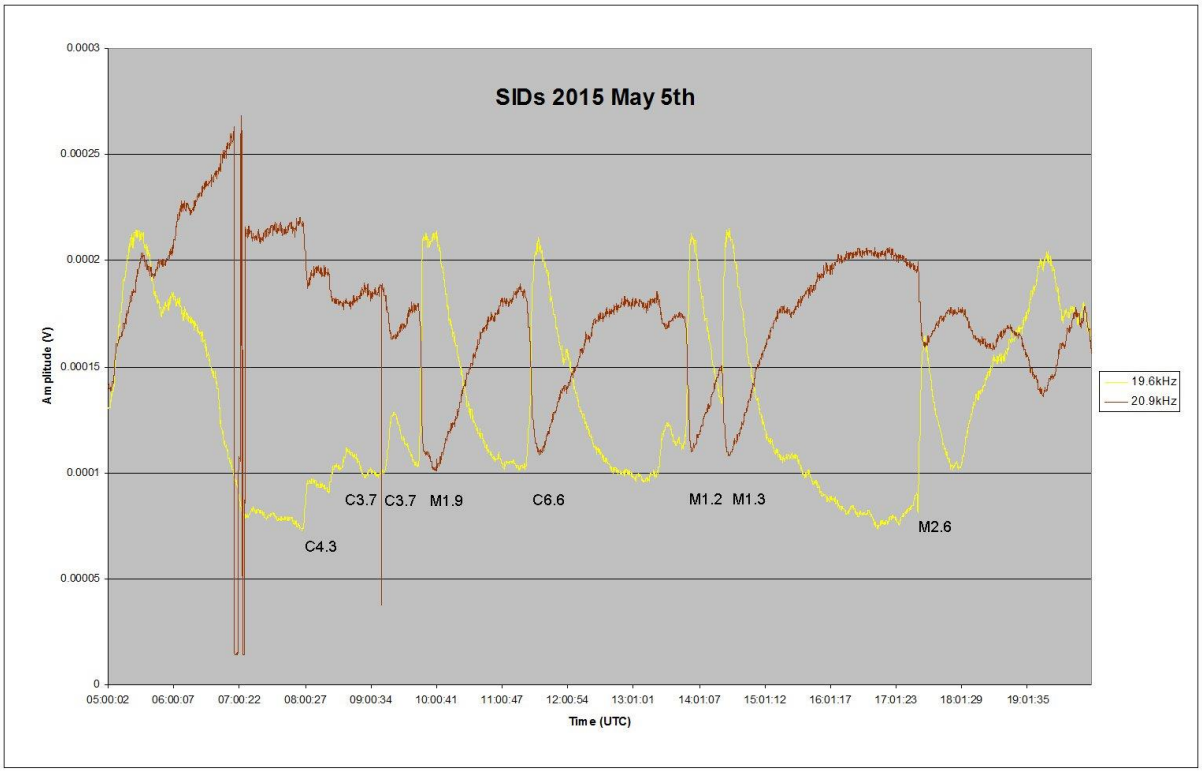

Fig 4: May 5th. Mark Edwards, Coventry.

Visual solar observers will have noticed some long filaments developing during May. One of these erupted on the 2nd, producing an Earth-directed CME. This was recorded as a SSC at 01:42UT on the 6th as shown in the recording by Colin Clements, Fig 5. The SSC shows as a small step in the X-field (red), and a transient in the Y-field (blue). A gentle disturbance continues through the rest of the day. No flare-derived CMEs were recorded, the remainder of May's activity being from coronal hole effects.

SID activity increased again in June with the presence of some larger and more complex sunspot groups. There were eight M-class flares, the most energetic being an M7.9 on the 25th. The 11th was particularly busy, observers recording a total of nine flares as SIDs. Most of these are shown in my own recording, Fig 6, at 23.4 kHz.

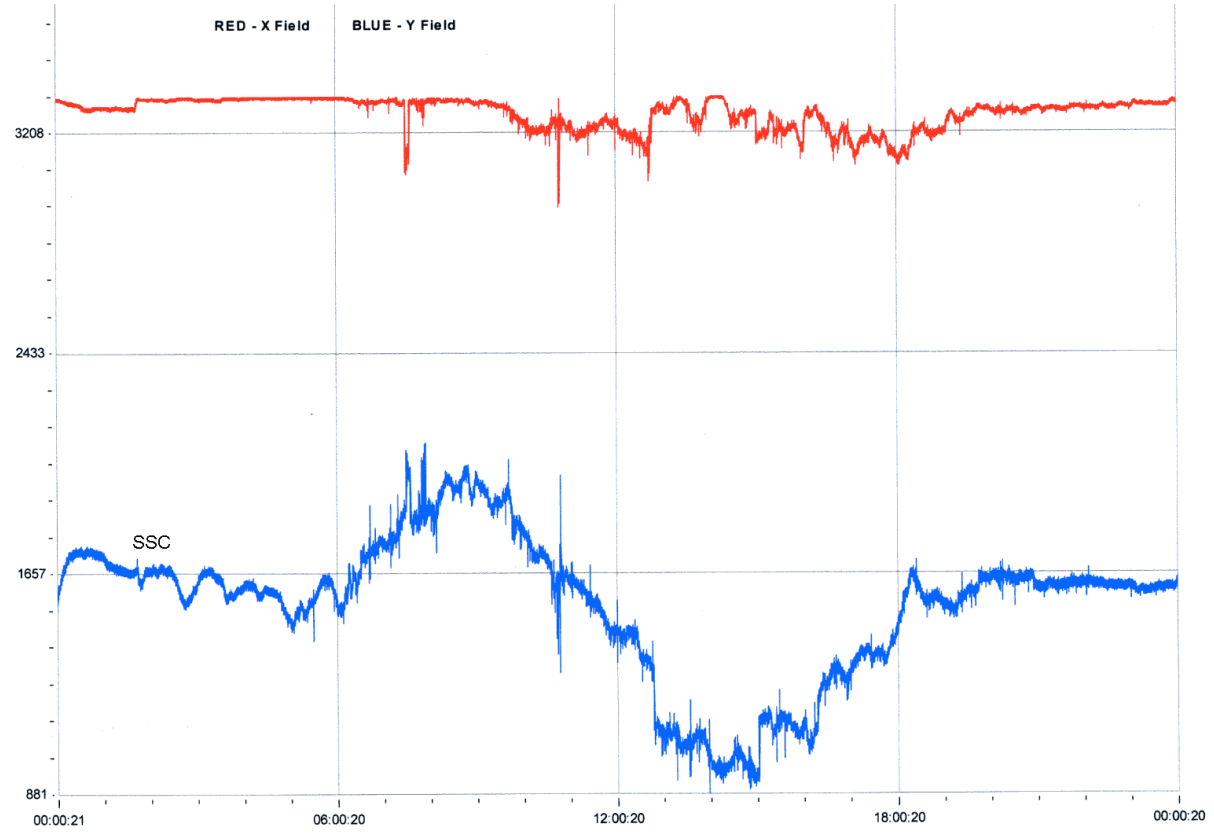

Fig 5: May 6th. Colin Clements, Lisburn.

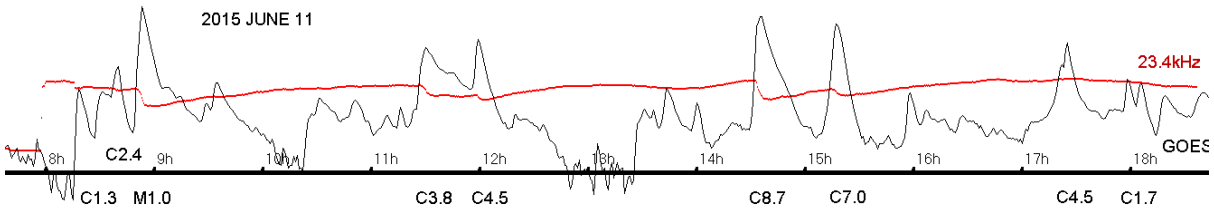

Fig 6: June 11th. John Cook, Wolverhampton.

Flare strength increased as the month progressed, with an M6.5 flare recorded at 18:02UT on the 22nd. This was followed at 20:05 by a widely recorded SID that did not have a matching solar flare. Fig 7 shows the SIDs recorded by Mark Edwards in the top panel, with the GOES X-ray data shown underneath in black. A small C3.9 flare is followed by the double-peaked M6.5 flare and a long decay until a further small peak at about 21:10. The VLF traces follow the C3.9 and M6.5 detail well, but are then suddenly interrupted by a further SID starting just before 20:00. The magnetic recording by Roger Blackwell is in the lower panel. It has been scaled to fit in with the other charts. A major magnetic disturbance can be seen starting at 18:30 in the Bx component (blue). By is red and Bz is green. A further sharp transient occurs just before 20:00, co-incident with the extra SID, the change in Bz being 350nT. Rapid changes in magnetic field cause large currents to flow in the ionosphere, and can therefore cause a rapid heating of the ionosphere. The warmer plasma will be more buoyant than its surroundings and would tend to rise.

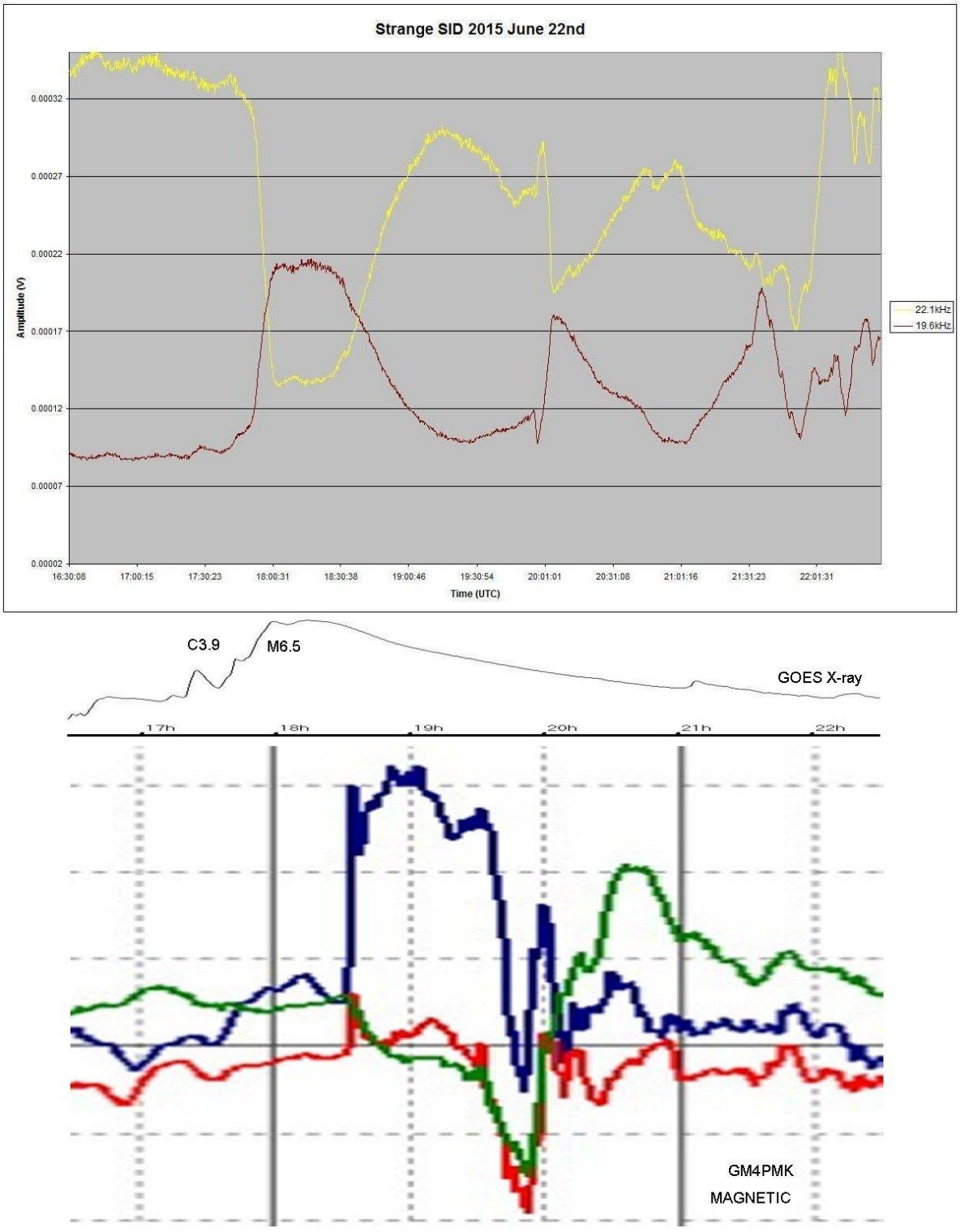

Fig 7: June 22nd. SIDs: Mark Edwards, Coventry. Magnetic: Roger Blackwell, Isle of Mull.

The SID could therefore be due to this rising volume of ionosphere altering the local electron density as if a flare had occurred. Unfortunately it was very close to local sunset, and no further VLF details are recorded. The magnetic disturbance may have been the result of a CME from a flare early in the morning of the 21st.

A small SFE was recorded at 09:40 on the 21st June, coincident with the M3.8 flare. The reverse of the effect described above, the rapid increase in ionisation has increased the currents flowing in the ionosphere and therefore caused a small magnetic disturbance. It measured about 6nT on my recording. The Bartels diagram in Fig 8 shows all of the magnetic activity together with flare magnitudes (C, M or X) for each day. Based on a 27 day cycle, there is a slight drift relative to the Carrington rotation number used by visual observers.

Observers: Roberto Battaiola, Jim Barber, Roger Blackwell, Colin Clements, Mark Edwards, Paul Hyde, Steve Parkinson, Phil Rourke, Gonzalo Vargas, John Wardle, and John Cook. My thanks to all contributors. If you would like to add your own observations, please contact jacook@jacook.plus.com.

August 2015

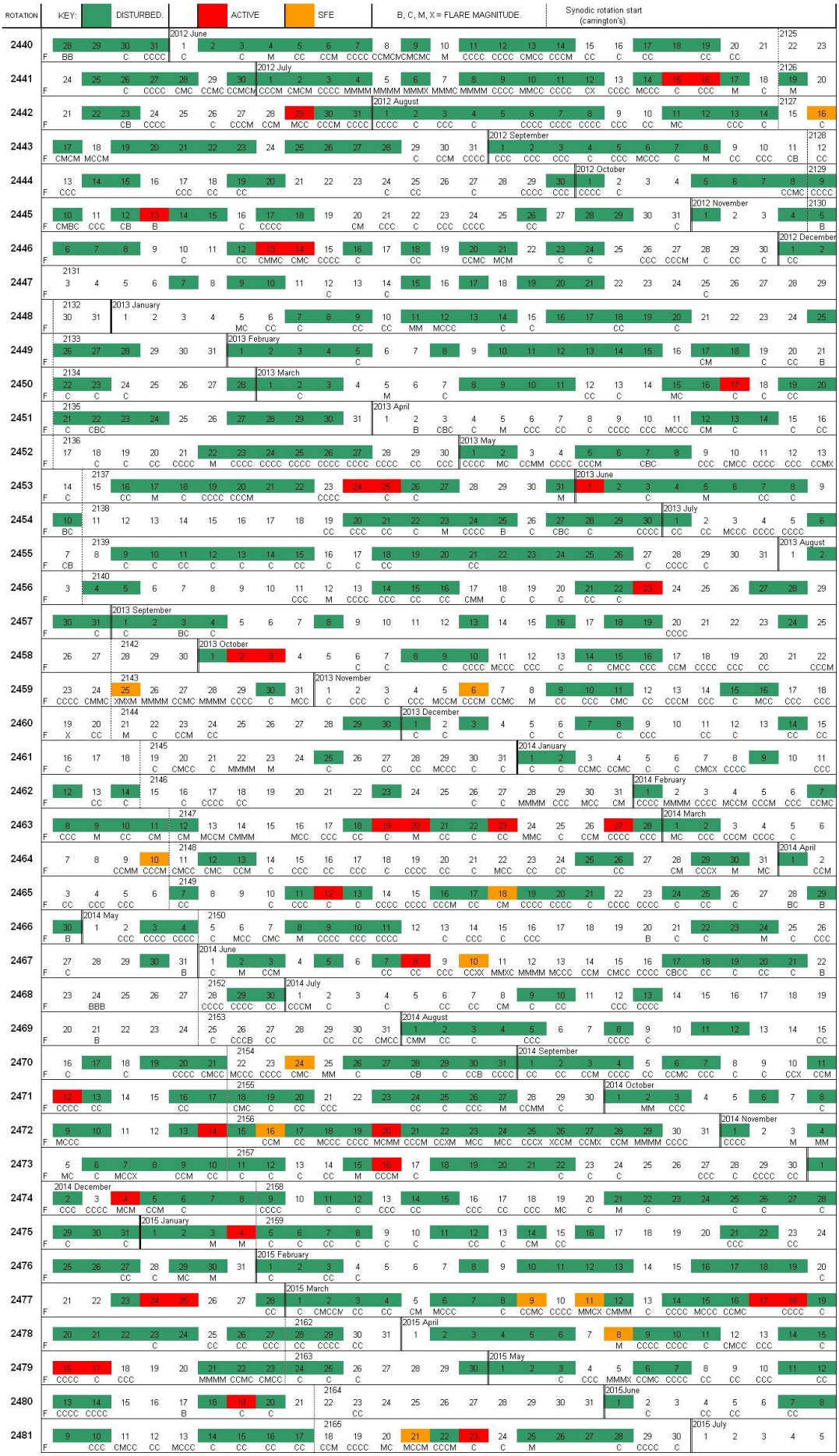

Fig 8 Bartel's Diagram

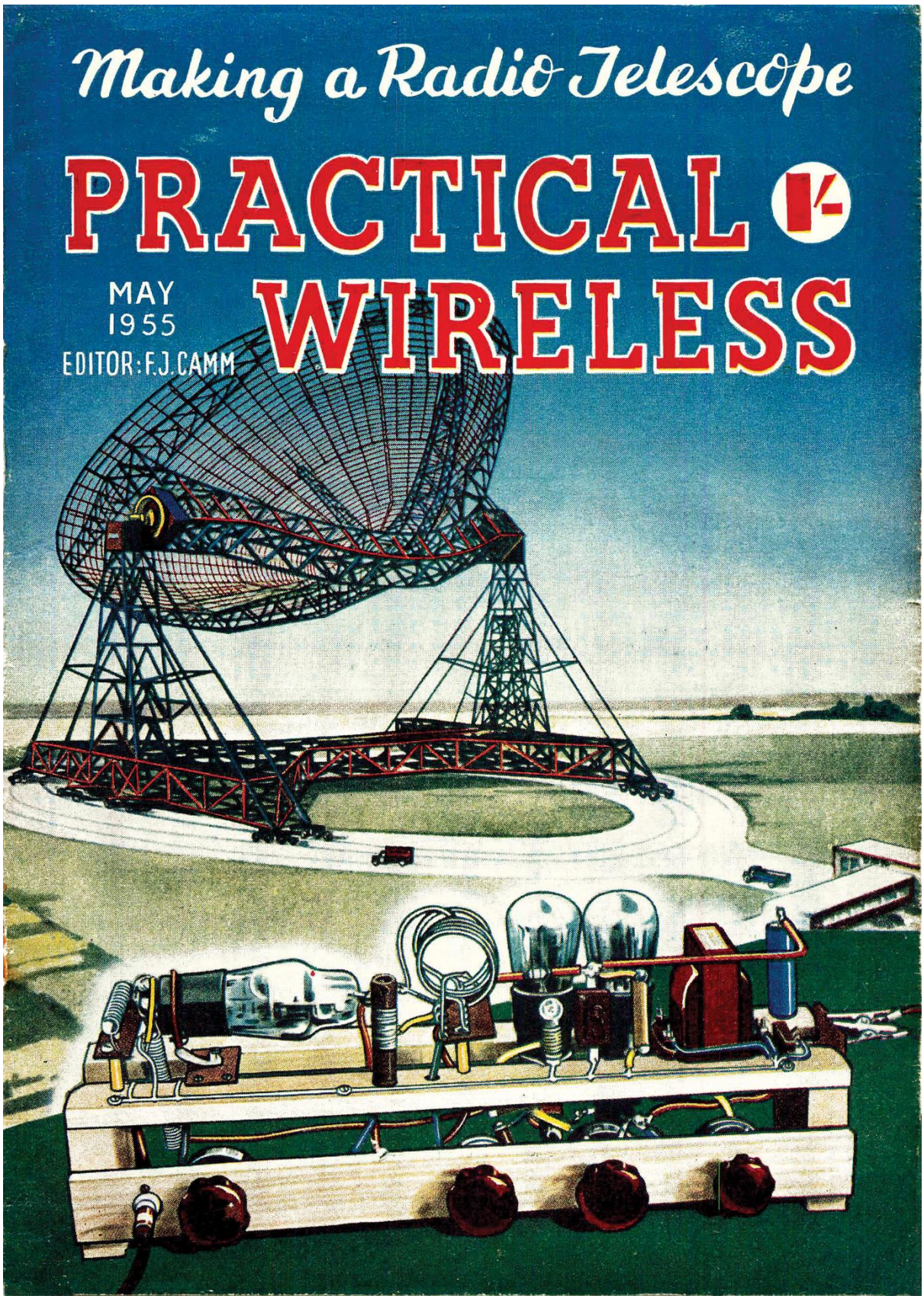
Making a Radio Telescope
PRACTICAL
1/-
WIRELESS
MAY
1955
EDITOR: F.J. CAMM

May, 1955 PRACTICAL WIRELESS 287

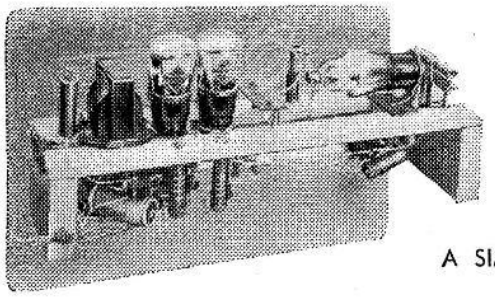

Making a Radio Telescope

A SIMPLE HOME-MADE BUT EFFICIENT INSTRUMENT FOR THE EXPERIMENTER

PART 1.—THE RECEIVER

By W. Schroeder

THE signals reaching us from outer space are weak, and detecting them and precisely measuring their strength calls for a very high degree of sensitivity of both the radio and the recording equipment.

As the average radio constructor is hardly interested in absolutely precise equipment—the results obtained with that could be appreciated only by an astrophysicist—the apparatus to be described here was designed with a view to simplicity in construction and operation without sacrificing an appreciable degree of sensitivity.

The intensity of the radiations reaching us from extra-terrestrial sources in the wavebands from 15 metres down to 1 centimetre is in the same region as the thermal noise generated by the aerial. The receiving apparatus, therefore, must have a very high amplification. It is also desirable to have a wide bandwidth in order to make a maximum of power available for detection. The signal-to-noise ratio should be as low as possible, and the equipment is preferably operated from a stabilised power supply, or from reliable batteries, to keep the gain at a constant level, and to make it possible to detect even small changes in the intensity of the received radiations.

Considering these requirements, the successful construction of a radiotelescope seems to be beyond the capabilities of an amateur. A T.R.F. receiver with sufficient gain has—of necessity—insufficient bandwidth, and the input of a superhet seems to be too noisy to be of any practical use.

A super-regenerative receiver can, however, easily be made to fulfil these requirements satisfactorily. It has sufficient bandwidth, extremely high gain, and its signal-to-noise ratio can be kept low enough to be employed usefully to detect the faint signals from the sun or the Milky Way.

The usual form of the super-regenerative receiver provides an output which is proportional to the logarithm of the signal strength, and the power indicated in the output circuit would be practically the same with, as without, a signal being present, as, in the latter case, the aerial noise will be amplified up to the same level as would the signal.

Many war-time radar receivers employed a super-regenerative circuit which is working in a linear mode, and it is this circuit which is the only practical solution for the amateur radio astronomer who constructs his own apparatus.

The Circuit

In Fig. 1 the circuit of a linear receiver is shown consisting of a super-regenerative oscillator, a quench oscillator, and the detector. The grid of the first oscillator is biased to a point where self-oscillation does not take place. The quench-oscillator produces

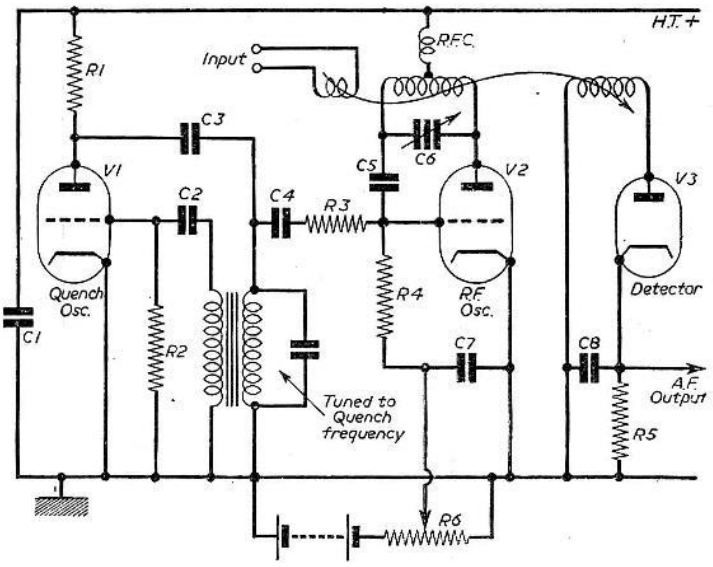

Fig. 1.—Basic circuit of super-regenerative receiver working in linear mode. V1—Quench oscillator, V2—Super-regenerative oscillator, V3—Detector.

List of Values

R1 = 50 K Ω
R2 = 10 K Ω
R3 = 100 K Ω
R4 = 100 K Ω
R5 = 25 K Ω
R6 = 100 K Ω (Variable)
C1 = 0.01 μF
C2 = 100 pF
C3 = 0.001 μF
C4 = 100 pF
C5 = 50 pF
C6 = 25 pF (split stator)
C7 = 0.001 μF
C8 = 0.001 μF

an alternating voltage which is superimposed on the steady grid-bias voltage.

During the positive parts of the quench-cycles, the super-regenerative valve becomes conductive, and oscillations begin to build up.

The exact moment when these two voltages cancel one another to the extent of making the valve conductive is the only part of the whole quench-cycle during which the receiver is sensitive either to signal or to noise. The signal (or noise) voltage then present determines the initial amplitude of the oscillations which afterwards build up to about one million times that value. Fig. 2 shows the envelope of the super-regenerative oscillations during one quench-cycle without and with a signal at the receiver input in relation to the grid-voltage at the oscillator.

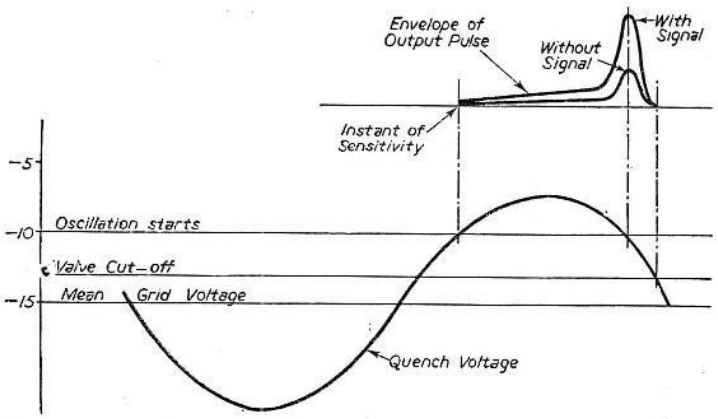

Fig. 2.—Shape of the output pulse envelope in relation to the voltage (bias plus quench) at the grid of the oscillator.

During the n gative parts of the quench cycles, the valve must be biased beyond the cut-off point to make sure that the oscillations cease ; otherwise the next burst of oscillations builds up from the remainder of the oscillations from the previous cycle, instead of from the signal, with consequent loss of sensitivity.

As the current required by the valve to start oscillation is only a fraction of the current passed by the same valve when used as an amplifier, the shot noise is considerably smaller, and the noise factor is decreased. This can be further improved by making the coupling very tight, thus further reducing the current required to start the valve oscillating.

The mean anode current of the oscillator increases during each burst of oscillation and, as the mean of the oscillation amplitudes alters with the signal strength, the anode current has a component at carrier modulation frequency which, in radio astronomy, is a random noise.

As the gain of a super regenerative receiver of this kind is proportional to the period of the quench cycle, this should be made as long as possible.

Five hundred cycles per second is by no means too low a frequency, and as the actual noise received is of no importance, it does not matter if the output is modulated by an audible frequency.

Gain is also increased by adjusting the grid-voltage of the super regenerative oscillator to a point where the peak amplitude of the oscillations in each burst comes as near saturation point as possible, but without actually reaching it. If it does, the set no longer works in the linear, but in the usual logarithmic mode. An oscilloscope connected to the output is the only means of

Radiotelescope as used l amplifier, R.F. oscillator. unit houses the

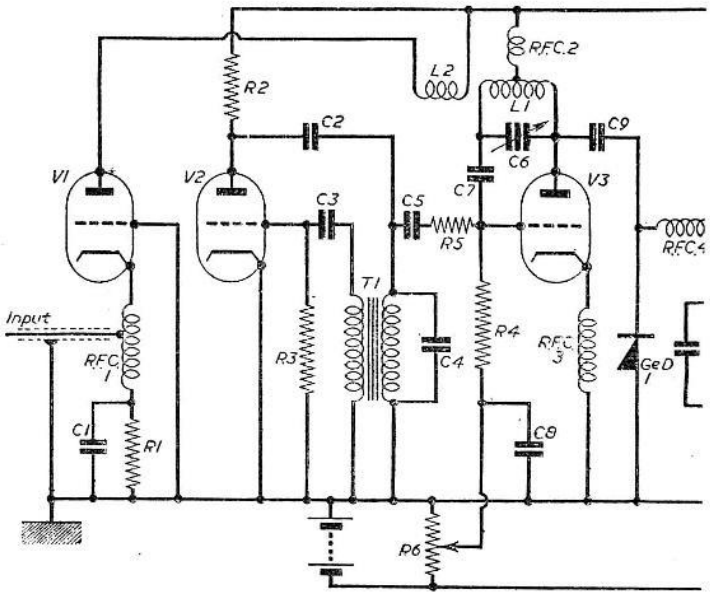

Fig. 4.—Circuit of the complete receiver consisting of grounded grid R.F. stage, L.F. crystal rectifier, an

making sure of this, and the oscillation envelope should have a shape as indicated in Fig. 2. On no account must the top of the curve be flattened down.

Finally, the gain is inversely proportional to the capacity included in the tuning circuit, and this should consequently be kept as low as possible. At the short wavelengths concerned, a few picofarads are all that is needed, anyway.

Taking all this in account, the super-regenerative receiver should have a gain of about 90 to 100 decibels.

R.F. Stage

If this receiver is connected to an aerial, it is liable to radiate oscillations which will interfere with neighbouring receivers, and which may be reflected by nearby metal objects and thus give misleading indications of received signal power. It is, therefore, necessary to precede it by an R.F. amplifier, which has the advantage of giving some improvement in the signal-to-noise ratio.

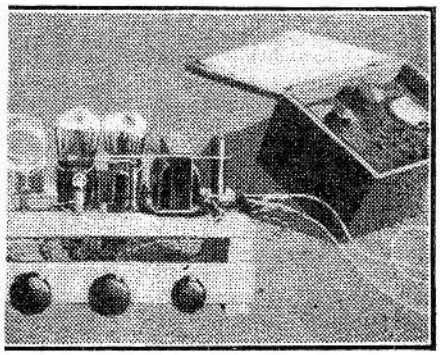

the author. The unit on the left contains R.F. quench oscillator and detector. The other L.F. amplifier and valve voltmeter.

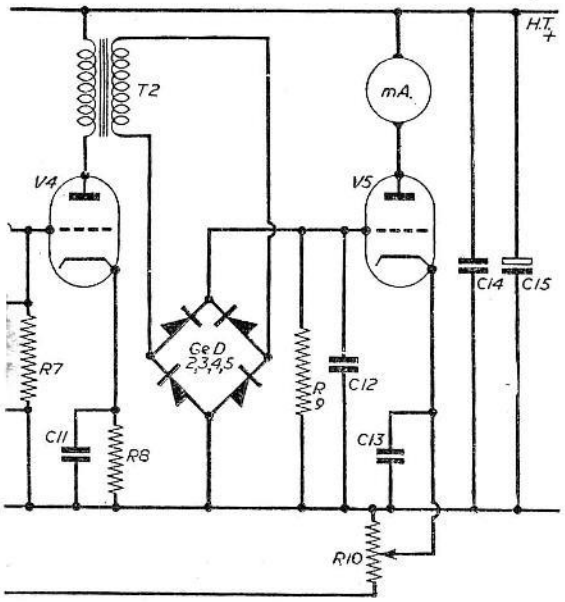

tage, quench oscillator, R.F. oscillator, crystal detector, L.F. valve voltmeter.

Unfortunately, it also destroys what is possibly the greatest advantage of the super-regenerative receiver in its application as a radio telescope: this is the advantage of single circuit tuning with its consequent bandwidth. The application of a grounded grid R.F. amplifier triode, however, avoids this complication, see Fig. 3.

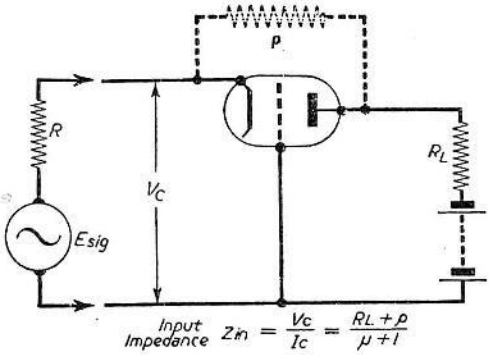

Fig. 3.—Basic diagram of grounded grid R.F. amplifier.

The output from the detector stage, which is either a silicon diode as used in radar receivers or a germanium diode capable of rectifying V.H.F.s, is amplified in a single-stage L.F. amplifier and then rectified by four germanium diodes in bridge circuit. These can be low-grade types, but must be reasonably well matched (Fig. 4). The output from the L.F. stage is, of course, a 500 c.p.s. frequency, the amplitude of which is determined by the strength of the received signal. The condenser C11 is, therefore, charged to a D.C. potential which is proportional to the signal.

The circuit associated with V5 acts like a valve-voltmeter, and the 0-1 mA meter in the anode lead gives an indication of the signal strength. Without an aerial connected to the set, the reading obtained will

LIST OF COMPONENTS

(Fig. 4)

R1—According to valve
R2—50 kΩ
R3—10 kΩ
R4—100 kΩ
R5—100 kΩ
R6—250 kΩ pot.
R7—100 kΩ
R8—According to valve
R9—100 kΩ
R10—250 kΩ pot.

C1—0.001 μF
C2—0.05 μF
C3—0.001 μF
C4—To tune secondary of T1 to 500 cps.
C5—0.001 μF
C6—25 pF (split stator tuning condenser)
C7—50 pF
C8—0.001 μF
C9—10 pF
C10—0.001 μF
C11—25 μF electrolitic
C12—0.1 μF
C13—25 μF. electrolytic
C14—0.001 μF
C15—8 μF electrolytic

correspond to the noise generated in the set itself, and although this consists of random voltages, the meter gives a comparatively steady reading, because it is damped by the circuit constants. The bias of V5 can be adjusted to give a reading of 0.01 mA (this is easier to adjust correctly than zero). After connecting the aerial the new reading obtained corresponds to signal voltage received plus noise generated by the aerial itself. By directing the aerial towards a part of the sky which is known to be practically free from radiations, the meter can again be adjusted to give a reading of 0.01 mA, and then any reading different from this is due to actually received radiations.

Because of the high amplification none of the readings will be completely steady; the needle will always fluctuate somewhat, but quite small signals still give a reading which it is possible to distinguish from these fluctuations.

Layout of the Receiver

While Fig. 4 shows the final circuit of the complete receiver, Fig. 5 is a diagram of a suggested layout. The whole receiver is mounted on two strips of wood, 1in. by ¼in. by 18in. long, which are screwed to the top of two blocks of wood 2in. by 3½in. by ½in. thick. A third strip of wood is screwed to the front and this carries all the adjustable controls. The whole chassis is given two coats of aluminium paint and is then ready for mounting the components.

The sensitivity of a receiver built along these lines is very great indeed. If a noise factor of 2 or 3 is obtained on the meter waveband—which is quite possible with modern U.H.F. valves—an input of only 10-14 watts gives a clear indication. With a receiver bandwidth of 1 Mc/s and an aerial gain of only 10, the greatest part of the Milky Way gives a clear indication of radiations. From some parts these are, under the conditions mentioned, about 10 to 20 times greater than the minimum detectable.

Individual "radio stars," or the sun under normal conditions, do not radiate enough power to give a reading on this receiver. Not even when extreme care has been taken to stabilise the gain of the receiver. But a method was discovered some years ago which increases the sensitivity several hundred or thousand times, and this has the added advantage of eliminating any instability in the gain of the instrument.

Increasing Sensitivity

Fig. 6 shows the modifications necessary to obtain this enormous sensitivity. V6 is a noise generator coupled to the receiver input by L3. The noise power generated can be adjusted by altering the filament voltage, but always working the valve at saturation point, that is, with the full high-tension on the anode.

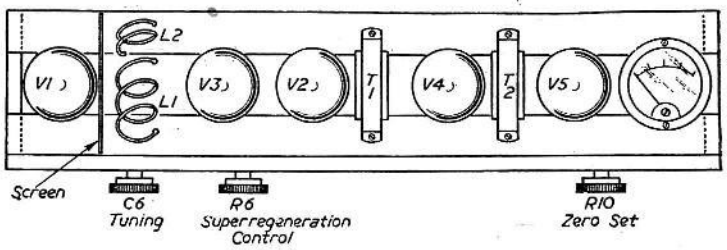

Fig. 5.—Suggested layout of receiver.

Two semi-circular aluminium plates rotate on a common shaft at a speed of about 25 rps, alternatingly coupling the aerial and the noise generator to the input. Any difference between the intensities of the received signal and the comparison noise appears as a 25 cps square-wave modulation in the output of V4 of the receiver.

This is mixed in a Cowan modulator (the four germanium diodes must be well matched to avoid cross-modulation) with another 25 cps square wave produced by the battery and the two brushes connecting a metal foil on the driving shaft of the plates, which make contact throughout the time the aerial is coupled to the receiver, and breaking it while the generator is coupled to it.

The receiver output is either in phase or 180 deg. out of phase with this square wave, and thus producing either an increase or a decrease of the D.C. voltage at the output of the mixer. This D.C. potential is measured by a valve voltmeter as in Fig. 4.

This arrangement eliminates any instability in the receiver, as now only the difference between two noise levels is measured, and it greatly increases the sensitivity.

(To be concluded)

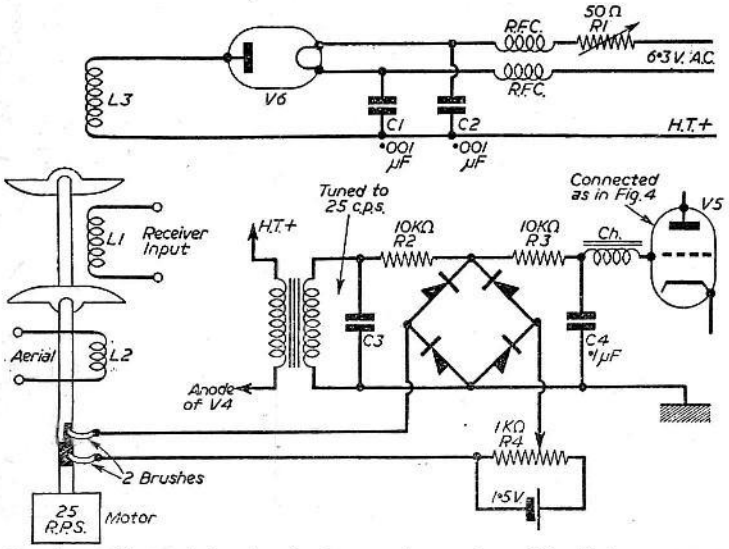

Fig. 6—Additional circuitry for increased sensitivity. V6—Noise generator.

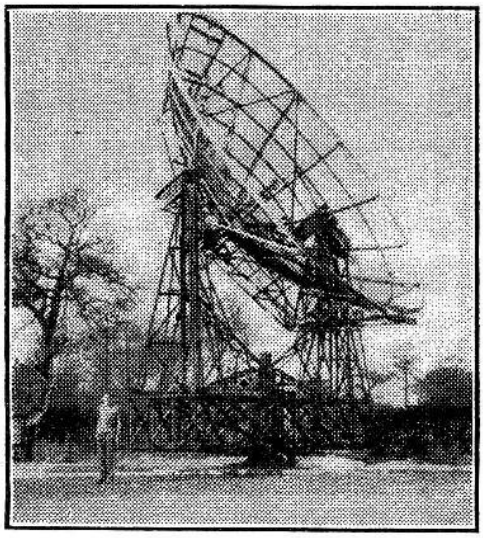

A completely steerable 30ft. parabolic reflector used as a radio telescope at the Jodrell Bank experimental station.

Making a Radio Telescope

A SIMPLE HOME-MADE BUT EFFICIENT INSTRUMENT FOR THE EXPERIMENTER

PART 2.—AERIAL SYSTEMS

By W. Schroeder

AN input which is only a minute fraction of the noise power generated in the receiver still gives a clear indication, and with this improvement it may be well worth while to connect an automatic recording instrument instead of the meter to the output. This can even be calibrated directly in units of field strength.

An aerial—in order to be usefully employed in a radio telescope—must be highly directional. To a certain extent this property is inherent with all types of aerials, but not nearly sufficiently for the purposes of radio astronomy.

Best known among the directional aerials, of course, is the usual television aerial, normally consisting of a half-wave dipole with a reflector placed behind it.

A simple dipole has a power gain of 1.64 over an aerial which receives at equal strength from any direction. Such a purely theoretical aerial is called an isotropic aerial and cannot be realised in practice. It is conceived merely as a standard for comparison.

For use in radio astronomy, however, aerials of considerably higher gain and directivity must be used. This can easily be achieved by using an array of several half-wave aerials and feeding them in phase (Fig. 1). Highest sensitivity is in the direction Z. The polar diagram of this four-element system is shown in Fig. 2. Sensitivity is zero at an angle of 30 degrees from the direction of the highest sensitivity (Z), and by increasing the angle a smaller maximum of sensitivity is found. These "side lobes" are present with all multi-element arrays.

The beam width of this aerial, which is reckoned to the angle at which half maximum sensitivity is measured (−6 db), is about 35 degrees. An eight-element system would have a beam width of 25 degrees, and by further increases the directivity can be made greater still.

If several such "stacks" are placed side by side, the directivity in the horizontal plane can be increased too. Such broadside arrays (Fig. 3) are used quite frequently in radio astronomy, and they are especially effective if a conducting screen, usually

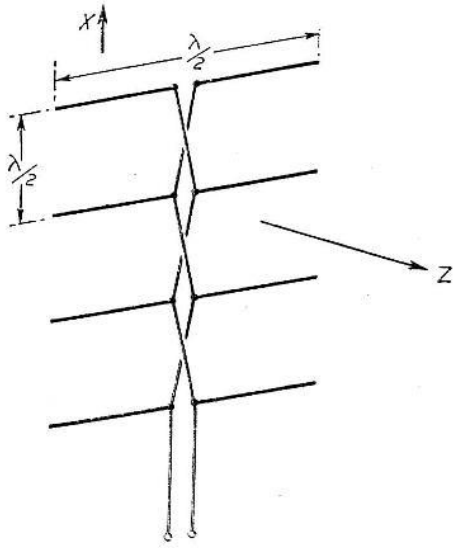

Fig. 1.—4-element stack of half-wave dipoles. In-phase feeding is achieved by crossing the feeders between elements.

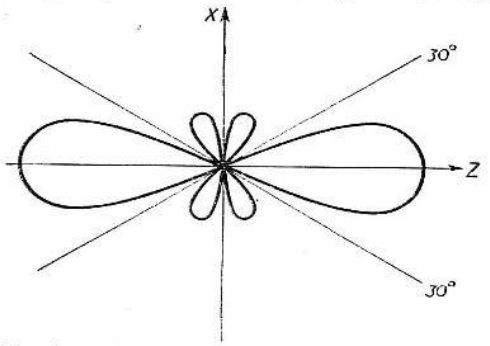

Fig. 2.—Polar diagram of a system of four half-wave dipoles. Highest sensitivity in direction Z, zero sensitivity in directions 30 deg. and 90 deg. (X).

consisting of wire netting, is placed one eighth of a wavelength behind the elements. This doubles the gain of each half-wave aerial, and the combined gain of the system in Fig. 3 would be 2 × 1.64 × 20 = 65.6.

The screen at the back should overlap the aerials by at least half a wavelength. The beam width of the array shown is about 30 degrees in any plane.

A more economical method, though a little more

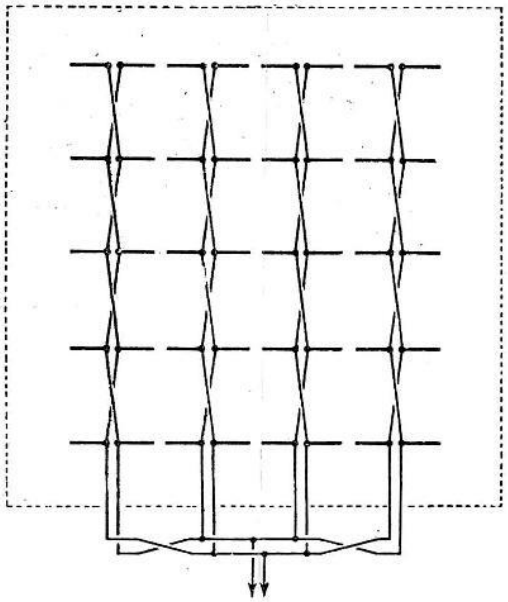

Fig. 3.—Graphical representation of a 20-element broadside array, with screen behind. Power gain about 66, beam width 30 deg.

difficult to construct, is the erection of an array of Yagi aerials. A single unit of this type, consisting of a folded dipole, a reflector 0.15 wavelength behind the dipole, and five directors, 0.434 wavelength long, and spaced at half-wavelength intervals in front of the dipole, has a gain of about 20 and a beam width of 35 degrees. The measurements given represent the optimum values found experimentally.

Five such systems can conveniently be mounted on a frame which should be as large as possible to keep the beam width small (Fig. 4). Working on a wavelength of about 1 metre, and the Yagi elements at the corners of a square with sides 20ft. long, the arrangement will provide a gain of 100 and a beam width as small as 10 degrees. (Beam width is approximately 60 wavelengths divided by length of the sides of the square. This formula also applies to broadside arrays).

Both broadside arrays and Yagi aerials, although extensively used in radio astronomy, have one great disadvantage: they have to be constructed for a specific wavelength, and any desired change of this requires a complete rebuilding of the aerial system.

Overcoming a Disadvantage

This disadvantage can be overcome by the use of a parabolic reflector. This usually consists of a circular frame over which a wire mesh is stretched in such a manner that a cross-section through the centre is a true parabola, and the dipole is situated at the focus.

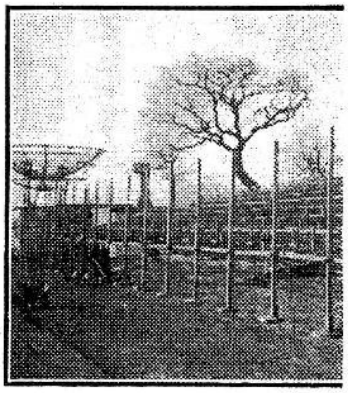

A partly adjustable broadside arr aeria

Theoretically such an aerial has a power gain of $\frac{4\pi A}{\lambda^2}$ where A = area of the aperture, and λ = wavelength. The spacing of the wire mesh introduces some losses, however. These amount to 20 per cent. if the wires are spaced $\lambda/10$ apart, and 35 per cent. if spaced $\lambda/8$. The latter is the widest practicable spacing.

An aerial system of 20ft. diameter, working on a wavelength of 1 metre, and with wires spaced 5in., would have a power gain of about 220, quite enough to feed our receiver and give useful indications of the radiations which reach us from the Milky Way. The beam width of the system would be in the region

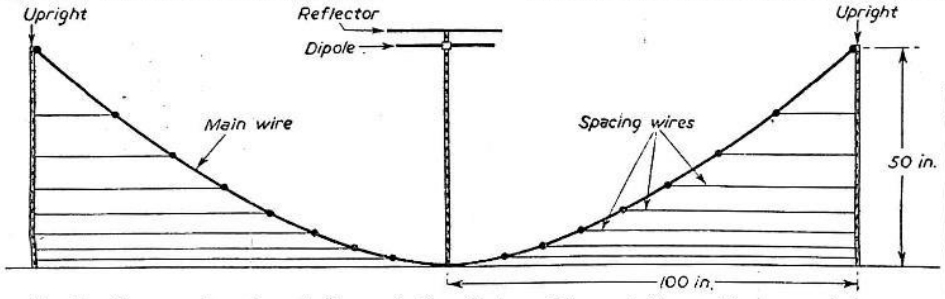

Fig. 5.—Cross-section through the parabolic reflector. The uprights can be secured by guy ropes. The measurements for the spacing wires are given in the table.

Distance fr
12.5i
25in
37.5
50in
62.5
75in
87.5
100in

of 10 degrees, quite a useful value for its intended application.

The construction of such an aerial is comparatively simple, especially if it is not required to be steerable. This need be no great disadvantage, as a certain amount of steering is possible by tilting the arm which carries the dipole at the focus. Without much deterioration of gain or beam width a deflection of up to 15 degrees can be achieved.

Aerial Construction

The framework can be constructed of metal or timber, the simplest method being a number of poles stuck in the ground. The height of the uprights must be one quarter of the diameter of the framework, and

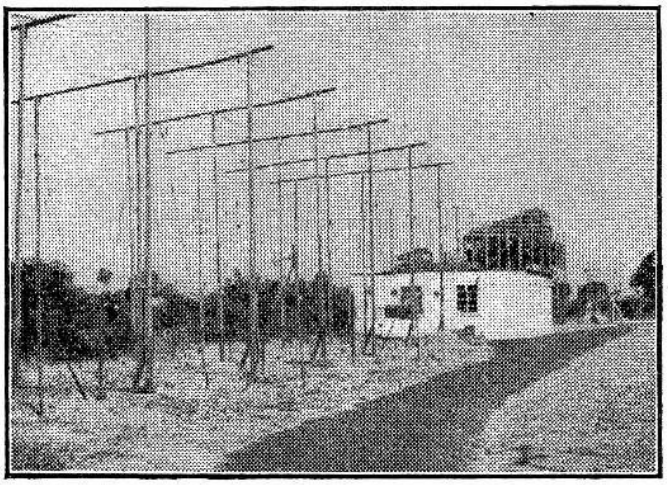

A fixed array of Yagi aerials for the reception of extra-terrestrial radiations.

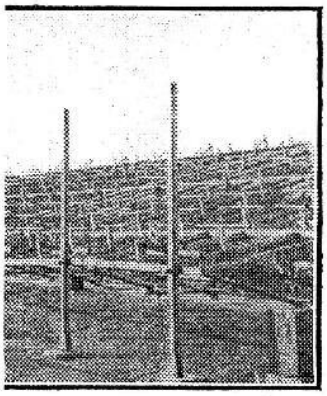

ty of several hundred half-wave ls.

the dipole at the centre is fitted at the same height. To make the shape of the reflector as near parabolical as possible, 12 uprights at least are necessary, but for larger systems working on shorter wavelengths, this number must be increased. At no point must the shape of the finished wire mesh depart more than $\lambda/8$ from the true shape of a paraboloid.

In Fig. 5 are shown the suggested measurements for such an aerial, showing two of the uprights which are opposite one another with the arm carrying the dipole in the middle, which it should be possible to tilt in a north-south dire ction.

In the centre, a wire ring is fitted, which should

Table 1

om centre.	Height from ground.
n.	1in.
.	3in.
n.	7in.
.	12.5in.
in.	19.5in.
.	28in.
in.	38in.
.	50in.

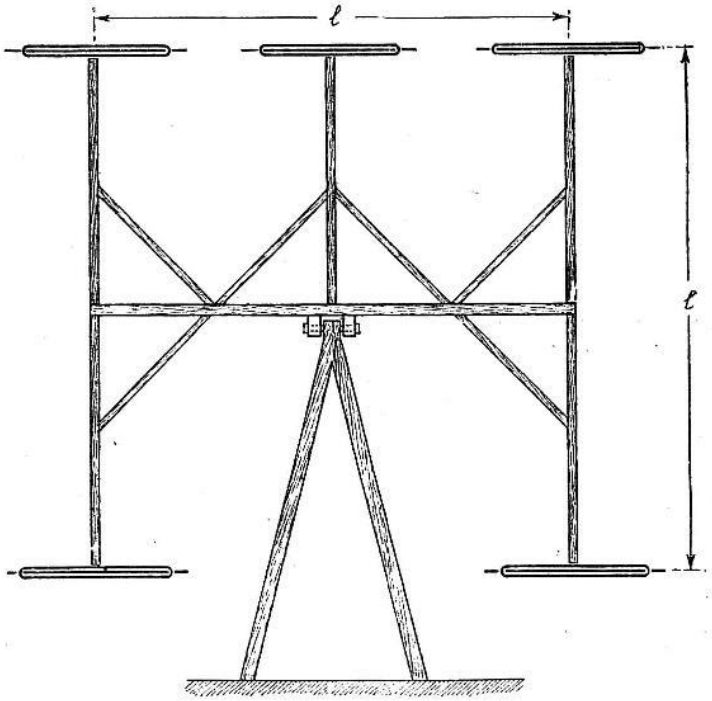

Fig. 4.—End-on view of an array of five Yagi-aerials. For l=20ft., and on a wavelength of 1 metre, the beam width is 10 deg., and the power gain 100.

have a diameter of 25in., and is fixed 1in. from the ground. Twelve wires are soldered to this ring, and their other ends are laid over the tops of the uprights, and weighted down to keep them taut. At a distance of 25in. from the centre, spacing wires are soldered to the twelve wires in such a manner as to keep the solder joints 3in. from the ground. Further spacing wires are then added according to the measurements given in the table.

For smaller or larger aerials these measurements must be decreased or increased in proportion.

When all spacing wires are in place, the ends of the twelve mains wires are fixed to the tops of the uprights, and they should then all be in the shape of parabolas.

Starting from the innermost ring, further rings are soldered to the main wires at intervals of 4in. Finally, another number of wires are soldered between the main ones, starting from that ring where the distance between the main wires just exceeds 4in., and carrying on to the rim of the " bowl," so that at no point of the completed mesh there is a space of more than 4in. between any two wires. A reflector built to these measurements can be used at wavelengths down to 70 cm. (420 Mc/s) and at that frequency would have a power gain of about 300. If the spacing of the mesh is reduced to 2in., the gain reaches nearly 500.

The dipole at the focus is best fitted with a reflector behind it, on the side away from the " bowl." Although this has little effect on the gain, it considerably reduces the side lobes of the system.

It is necessary to match the aerial fairly accurately to the receiver input, as any mismatch not only results in a loss of power, but also introduces additional noise in the aerial, as the lost power is used to produce a thermal noise, and as the strength of this would not be constant it would lead to inaccurate indications.

If the aerial is built on level ground the beam is directed towards the zenith, and the measurements of the receiver therefore relate to that part of the sky which is right overhead at the time of observation. As the Milky Way at certain times during the day reaches this position, fairly strong signals will be recorded. The radio telescope can be kept running all day long, and if it is made self-recording, a graph will be obtained showing the strength of radiations reaching us from different parts of the sky. These measurements can be compared with those taken on other days, but on the whole it will be found that the field strength recorded will be the same for any particular part of the sky.

By tilting the supporting arm of the dipole, the beam is displaced, and another part of the sky can be investigated. In each position, the beam sweeps out another circular strip of the sky, about 10 degrees wide, as the earth makes one revolution with regard to the fixed stars. When the possibilities of the aerial have been exhausted, the change to another wavelength offers new scope.

Hydrogen gas, which is fairly common in outer space, emits under certain conditions a strong radiation on a wavelength of 21 cm. The recording of this radiation and of the Doppler-shift associated with it has led to the most important results achieved by radio astronomy. So far, no other such " spectrum lines " have been discovered, but they should, theoretically, be present on some longer wavelengths. Here is a field of research for the keen amateur.

As " new stars " and other surprises in astronomy are almost always discovered by amateurs working with quite small telescopes, it is not impossible that in radio astronomy unexpected changes or developments are to be also first noticed by an amateur, in spite of the watching eyes of the scientists of Manchester University, who, at the end of this year, will take into use a new radio telescope of 250ft. diameter.

Correction

In the first column on page 290 of last month's issue it was stated that the receiver would give certain results with an input of only 10-14 watts. This figure should, of course, have been 10^{-14} watts.

Editor's note: While the following review has nothing directly to do with radio astronomy. I think we would all agree the influence Patrick Moore has had on many of us. He has inspired so many of us to get involved over the years.

Radio Play Review: Far Side of the Moore

by Sean Grundy.

BBC Radio 4

Reviewed by Martin Edmonds

Monday 30th March saw BBC Radio 4 broadcast a new play by Sean Grundy entitled 'Far Side of the Moore'. This 45 minute programme starred Tom Hollander as Patrick Moore with Patricia Hodge as his mother Gertrude. The play is available to download for a limited period and I certainly hope it will receive a CD release too.

Starting in 1957 when Moore's 'Suns, Myths and Men' had received a critical mauling in the BAA Journal from Dr Henry King, Patrick is first heard in a state of despair and braced for more bad news when he is offered the role of presenter on what was to become The Sky At Night. The play follows the preparation and recording of that first programme, Patrick's fears and his preoccupations.

Mr Grundy has clearly read and studied Martin Mobberley's definitive biography of the great man, 'It Came from Outer Space Wearing an RAF Blazer!' (2013) because the play shows a great awareness and understanding of Moore's life and experiences. The script shows a genuine affection for Moore and makes innumerable subtle references to aspects of his life including several appearances from Arthur C Clarke, his mother painting the pictures that would eventually be published as 'Mrs Moore in Space' (1974) and the notorious incident with the fly during the first programme. References to the fact that the BBC's original choice of presenters for an astronomy programme were Frankie Howerd and Sabrina and the correct names being given for production staff merely highlight Mr Grundy's attention to detail and clear respect for his subject.

Tom Hollander gives a superb central performance as the young, middle aged and elderly Moore; his fast paced delivery clearly evoking the early years whilst his characterisation of the elderly Patrick delivers the slower, slurred delivery so familiar from those final difficult broadcasts.

Director Dirk Maggs and producer David Morley have more than done justice to Sean Grundy's play with a beautiful production that is fast paced without feeling rushed and a charming use of Moore's own compositions as incidental music, (Moore Music CD - 2001).

The play is kind to Patrick regarding his reminiscences of a war-time fiancée; Lorna. Whilst Mobberley has questioned her existence, here she becomes a central character in Patrick's imagination and dreams. The play is by turns funny, engaging and moving; the final lines depict a very elderly Patrick daydreaming about his broadcasts, how far into space the signals may have travelled and what might have been if Lorna had not died in a Nazi air-raid.

It is 9th December 2012, his last day on Earth, and he is ruminating about his record breaking achievement of presenting The Sky At Night for 55 years – a milestone with which he appears to be less impressed than impressed.

The last two lines of the play are worth quoting as they are a worthy tribute to both Patrick Moore the astronomer and Patrick Moore the man. The dream figure of Lorna informs him that:

"There are incredible leaps made every day in astronomy because you inspired so many children to look up at the sky – a generation of scientists are standing on your shoulders."

Whilst the elderly Patrick replies:

"That's good – it's an old suit anyway."

A beautiful play and a fond tribute to a great man; I recommend you track down a copy.

Improving meteor event accuracy in Spectrum Lab

Paul Hyde

Spectrum Lab is a versatile audio analysis package developed by Wolfgang Buescher and freely downloadable from the Internet. Uniquely, Spectrum Lab has an Interpreter function which provides the ability to measure and capture various aspects of the signal using a Conditional Actions (CA) script. This supports the automatic detection of meteor events and the recording of the start time, strength and duration of the meteor reflection, plus capture screenshots to provide a visual record for later checking.

Several internet resources carry examples of CA scripts for meteor scatter work, some simple and others that are more sophisticated. The key feature is the condition for identifying the start of a meteor event, which then drives the remaining actions. The usual method is to monitor a number of FFT frequency 'bins' within a specified frequency range and fire the trigger if the maximum of these values exceeds the average noise level across all of the bins, plus a configurable margin, for example 17 dB. This method is very good at excluding broadband noise spikes that would otherwise generate false triggers.

Table 1 lists the typical Conditional Actions statements found with this approach:

If	**Then**	**Comment**
always	A=noise(low,high): Sig=peak_a(low,high): Freq=peak_f(low,high) h2=str("hh:mm:ss",now)	Continually monitor the FFT frequency bins between the specified 'low' and 'high' frequencies
Sig>(A+17)	C=C+1: timer0.restart(2)	If the trigger condition is met, increment a duration counter and restart a 2 second timer
C=1	Mtime=h2:MName="Meteor"+h1: MSig=Sig:MFreq=Freq:MNoise=A	Transfer the start time, signal and noise levels and frequency to holding registers
timer0. expired(1)	E=E+1: fopen2("c:\\Spectrum\\"+"event_log"+ str("YYYYMMDD",now)+".txt",a): fp2(Mtime+","+str(E)+","+str(MSig)+","+ str(MNoise)+","+str(MFreq)+","+str(C)): fclose2:C=0	Once the trigger condition has not been met for 2 seconds, increment the event counter and save the initial start conditions and the event duration to a log file

Table 1 Traditional trigger sequence for recording meteor scatter events in Spectrum Lab

However, if you import the resultant text file into a spreadsheet and chart the difference between the Signal and Noise figures recorded for each event you find some odd results.

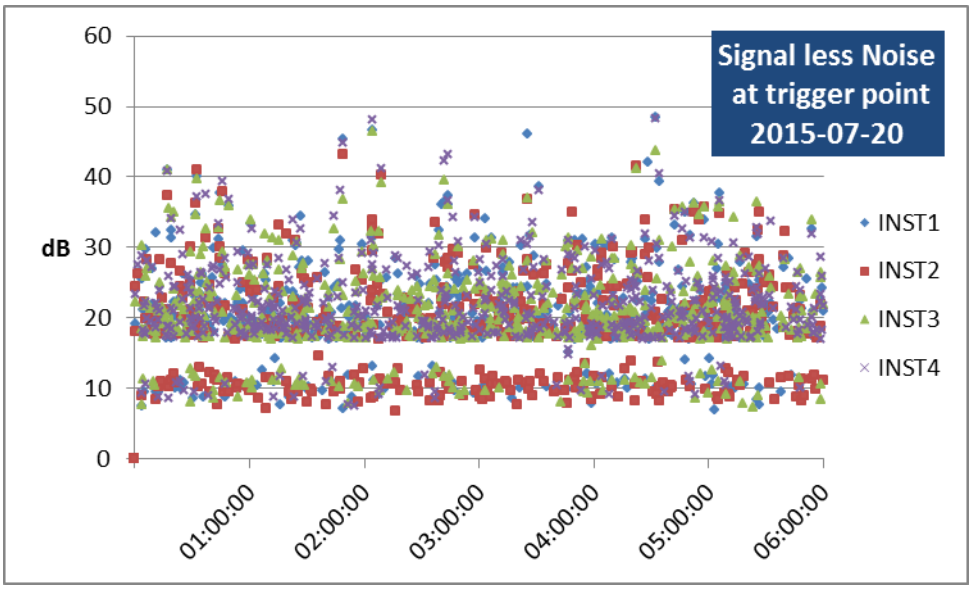

Figure 1 Recorded difference between Signal and Noise levels at the trigger point

The trigger test in the CA script is that the maximum signal within the defined Low to High frequency range exceeds the background noise by (in the example given) 17 dB. So no event should have a difference of less than this. However Fig 1 shows several events where the difference between the Signal and Noise levels is around 9 to 15 dB, which should not have generated a trigger.

If you chart the frequency associated with each trigger you find that valid triggers are associated with frequencies clustered around the GRAVES frequency (4400 Hz for my particular setup) plus a few events exhibiting high Doppler shifts, which is what you would expect. However the 'illegal' triggers return a random frequency lying anywhere within the specified Low to High frequency range.

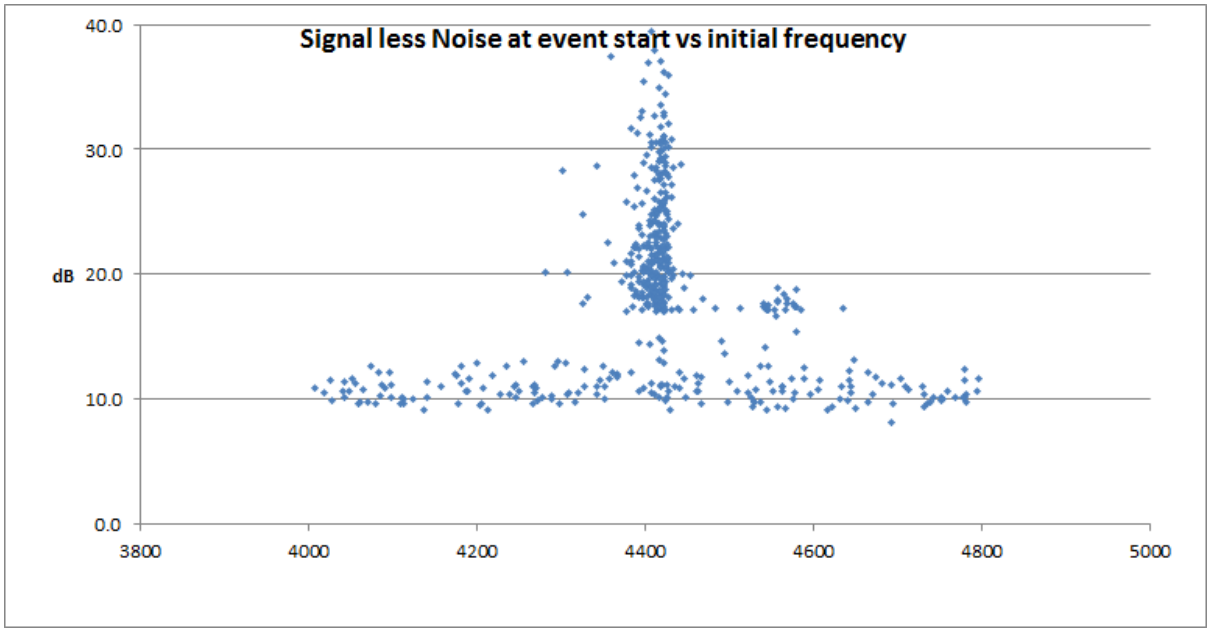

Figure 2 Difference between Signal and Noise levels versus recorded frequency (Hz)

Further analysis reveals that these illegal triggers are predominantly associated with very short duration events, where the trigger condition is met for just one FFT calculation.

Wolfgang Buescher has been very helpful in identifying the cause of these discrepancies, which is down to the FFT calculation running in a different software 'thread' to that of the Conditional Actions script. The trigger fires correctly when one of the FFT bins exceeds the defined Noise plus Trigger margin, but by the time the CA script comes around to shifting values into the registers, a new FFT calculation has taken place. For a long reflection event the values will be similar, but for events of less than half a second the FFT bins now only contain the tail end of the event or even just the background noise signal.

To overcome the problem, Wolfgang has introduced a new Interpreter feature:

"I have added a new event ("new_spectrum") to the conditional actions, which can be used to synchronize the script with the operation of the spectrum analyser. The entire CA script is then called immediately after a new FFT has been calculated, regardless of the configurable CA interval (in milliseconds). This way, the CA script won't miss a single FFT calculation, no matter how fast the waterfall display runs."

Combining the use of the 'new_spectrum' with that of the 'time' function, which gives the precise time of the FFT calculation, rather than 'now' which is the more general system time, ensures that the correct parameter values are saved to the log file. It also enables the time for which the trigger condition is met to be expressed in seconds rather than as loop counter, where the loop time will be dependent upon the specification of the host computer.

Table 2 illustrates the use of this technique and Appendix 1 contains a full CA script currently under test.

If	**Then**	**Comment**
new_ spectrum	A=noise(Low,High): Sig=peak_a(Low,High):Trig=(A+Level):	Use new command to force CA script to run after each FFT calculation
Sig>Trig & E=0	then S=1:E=1:inc(MCount):t1=time:	New event – use 'time' to record FFT time rather than 'now'
continuation	Event=MCount: TrigTime=str("hh:mm:ss",time): TrigSig=Sig:TrigNoise=A: TrigFreq=peak_f(Low,High)	Transfer trigger values to 'holding' registers
Sig<=Trig & S=1	then t2=(time-t1):S=0	Signal falls below trigger point so calculate duration

Table 2 Revised CA script using the 'new_spectrum' command

Figure 3 shows the results of four 'instances' of Spectrum Lab running on the same computer and monitoring the same receiver input. This time there are no events with Signal – Noise levels of under 17 dB.

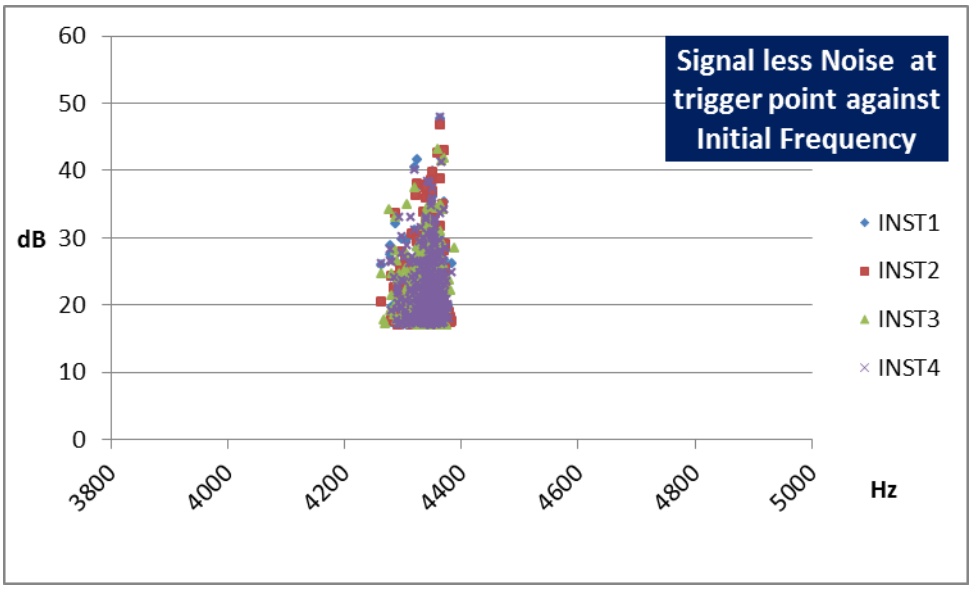

Figure 3 Signal less Noise versus frequency, utilising the revised CA script

Using the 'new_spectrum' command thus removes a systemic error affecting the recording of short duration meteor scatter events which records incorrect values for the signal strength and associated frequency at the trigger point.

Appendix A Conditional Actions script for meteor scatter observing

The following script is currently under test. It will need modifying to reflect the frequency at which the zero Doppler-shifted GRAVES reflections occur. I utilise a FUNcube Dongle Pro Plus receiver set at 143.046 MHz to minimise noise and which has a 350 Hz manufacturing offset, placing the GRAVES transmissions at 4350 Hz. The script saves a screenshot every 5 minutes to provide a complete visual record of activity so that false triggers can be identified and deleted from the event log file. This will fill up a hard drive and hence require regular archiving or deletion of the accumulated images.

If	Then	Comment
Initialising	Low=4100:High=4500:Level=17	USER to set Trigger frequency range (in Hertz) and Trigger Level (dB above noise level)
Initialising	timer1.periodic(300)	USER to set # of seconds between screenshots. Screen scroll rate should match this value.
Initialising	TrigTime=0:Event=0:TrigSig=0: TrigNoise=0:TrigFreq=0:MDurn=0.0	Clear event_log registers at startup
Initialising	R=0:S=0:E=0	Clear STATE flags: R = System running; S = Signal present; E = Event in Progress
Initialising	t1=0.0:t2=0.0:t3=0:MCount=0:Trig=0: timer0.restart(2):timer3.start(5)	Clear internal flags/registers and set start delay
Always	h1=str("mmss",now)	to support end of hour reset of MCount/Event
timer3. expired(1)	R=1:sp.print("SYSTEM START"): fopen2("c:\\Spectrum\\"+"event_log"+ str("YYYYMMDD",now)+".txt",a)	Start system/Open Event Log file
Continuation	fp2("Time(UT)"+","+"Event#"+","+"Sig(dB)"+","+"Noise(dB)"+","+"Freq(Hz)"+","+"Durn(secs)")	Save file header
Continuation	fclose2	
new_ spectrum	A=noise(Low,High): Sig=peak_a(Low,High):Trig=(A+Level)	Calculate new values after each FFT for trigger comparison
(R=1)& (Sig>Trig)& (E=1)&(S=1)	timer0.restart(2)	An event that is continuing from a previous trigger

If	Then	Comment
(R=1)& (Sig>Trig)& (E=1)&(S=0)	t1=time:timer0.restart(2)	Same event continuing after momentary break so register new start time
(R=1)& (Sig>Trig)& (E=0)	S=1:E=1:inc(MCount):t1=time: timer0.restart(2)	New event - record start time and initiate Timeout
continuation	Event=MCount: TrigTime=str("hh:mm:ss",time): TrigSig=Sig:TrigNoise=A: TrigFreq=peak_f(Low,High)	Transfer values at trigger point to 'holding' registers
(R=1)& (Sig<=Trig)& (S=1)	t2=(time-t1):MDurn=(MDurn+t2):S=0:	Signal falls below trigger point so calculate duration and add to accumulator
(R=1)& (timer0. expired(1))	E=0:S=0: sp.print(" Meteor ",Event," Dur",str("#0.0",MDurn)	Event ended. Add Event No and Duration to screen
continuation	fopen2("c:\\Spectrum\\"+"event_log"+ str("YYYYMMDD",now)+".txt",a):	Open Event Log file
continuation	fp2(TrigTime+","+str(MCount)+","+ str("#00.0",TrigSig)+","+ str("#00.0",TrigNoise)+","+ str("0000",TrigFreq)+","+ str("##0.000",MDurn))	Save to file
continuation	fclose2:MDurn=0.0:t1=0.0:t2=0.0	Close event log and reset registers ready for next event
timer1. expired(1)	capture("c:\\Spectrum\\screenshots\\" +"event"+str("YYMMDDhhmmss",now) +".jpg",75)	Save a screenshot to build up a complete visual record of activity

If	Then	Comment
val(h1,"####") =5959	t3=t3+1	
t3=1	MCount=0	Events in progress at hour rollover will be numbered against previous hour
val(h1,"####") =0000	t3=0	

Is there anybody out there?

EAARO to seek extra-terrestrial signals

Jonathan Blay

Following last month's announcement by physicist Stephen Hawking and entrepreneur Yuri Milner of the $100 million Breakthrough Listen project to dramatically boost the scientific search for signs of intelligent life beyond Earth, EAARO can report that we are exploring some of the novel ideas of cosmologist and EAARO patron Paul Davies to develop a complementary project to seek signs of extra-terrestrial intelligence.

Davies has argued that the search should look and listen for the techno-signatures of astro-engineering, interplanetary mining and spacecraft propulsion systems that might be expected in advanced civilisations. Another of Davies' ideas is that signals from an extra-terrestrial civilisation are likely to be broadcast as a beacon sweeping cyclically like a lighthouse rather than be directed specifically towards the Earth. He recently told Nature "I think SETI needs to revise its strategy and point its telescope towards the centre of the Galaxy for many years to maximize the chance of picking up such a transient signal."

EAARO will be pursuing Davies' approach in developing its project. While the details are still a work in progress, EAARO already has available a suitable site for the planned new radio detection facility, in the shape of a field in the heart of East Anglia's Fenlands.

Unlike most observational facilities EAARO will be able to search for extra-terrestrial signals 24/7 with no queuing for telescope time. This is one of EAARO's unique selling points.

In the meantime, EAARO continues to make progress in its other projects, including an advanced meteor radar system. Experiments are underway in the development of a pulse generator and amplifier, and tests have been undertaken using directional antennae. We expect to have some exciting news and will provide more updates in the coming months.

~~~

EAARO is a scientific and educational charitable company establishing a new radio observatory and ground station near Cambridge, UK, to use space exploration to encourage and inspire people to pursue interests and careers in Science, Technology, Engineering and Mathematics (STEM). For more information, visit our website at www.eaaro.org.uk. Contact us on Twitter @eaaro or via email at info@eaaro.org.uk.
~~~

August 2015

Amateur Pulsar Detection Using the RTL SDR

PW East (UK), GM Gancio (Argentina[1])

Introduction

This project sought to determine the minimum useful antenna aperture for amateur radio astronomers to successfully detect pulsars around the Hydrogen line frequency of 1420MHz. The technique relied on the collaboration with GM Gancio, who provided RTL SDR data of the Vela pulsar (B0833-45, J0835-4510) and others, collected with a 30m radio telescope. This data was processed to determine the achievable signal-to-noise ratio from which, the minimum useful dish size necessary for some effective amateur work, could be calculated. Two software packages were developed to do synchronous integration, a third to provide a power detection function and a fourth for spectrum analysis to recover pulsar rotation rate.

Pulsar Detection

Pulsar signals are very weak bursts of noise over a very wide frequency range at a regular rate. The duty cycle is typically 5-10%.

The detection process uses recorded complex IQ voltage sampled data collected at a chosen clock frequency f_c over an RF bandwidth equal to $B = f_c$.

The receiver input terminal noise voltage is proportional to, $\sqrt{k(T_p + T_{sys})B}$ within the pulsar pulse and $\sqrt{kT_{sys}B}$ outside. T_p and T_{sys} are the effective pulsar and receiver system equivalent noise temperatures.

Squaring the I and Q components (square-law detection)*, the result is (Figure 1) both DC components, $kT_pB + kT_{sys}B$, $kT_{sys}B$ in and out of the pulse respectively plus AC noise components, of similar magnitude, $kT_pB + kT_{sys}B$, $kT_{sys}B$.

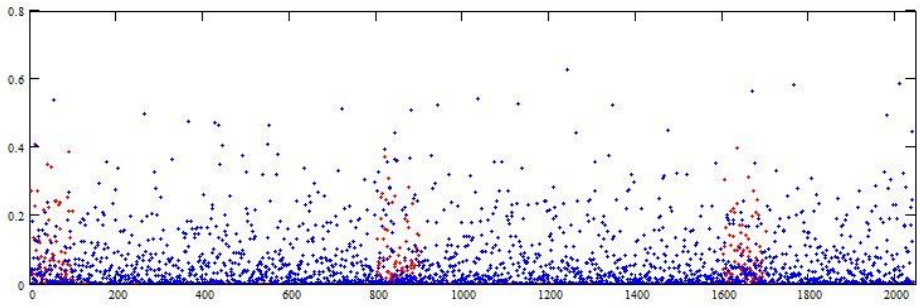

Figure 1 Square-law Detection v Time; System noise (blue) + Pulsar noise (red)

* Linear detection produces the same result if $T_p << T_{sys}$

The situation is depicted in Figure 1 showing unipolar system and pulsar noise from which the DC and AC components can be anticipated. Considering the DC terms, these appear as a weak pulsar pulse train sitting on the strong DC platform set by the detected system noise. To recover the DC pulse waveform from the high level AC noise, the technique is to synchronously add the pulses within the pulsar period. Synchronously summing *N* pulsar periods increases the DC voltage part by *N* and the AC term by $\sqrt{N}$.

The result is an improvement in pulsar signal-to-noise (voltage) ratio by $\sqrt{N}$ or,

$$SNR_v = \frac{\sqrt{N}T_p}{T_{sys}}$$

The programs *rapulsar* and *rapulsan* carry out this synchronous integration, requiring the pulsar rotation period measure to be chosen accurately.

The integration process sums the pulsar sampled data within its period divided in a number '*n*' of bins. The choice of bin number '*n*' affects the factor '*N*" controlling the SNR improvement.

If data is collected over a time 'τ', then $Nn = \tau\ f_c = \tau B = F$; equal to the data file number of samples, *F* as set in *rtl_sdr* command line,

$$\text{or,}\quad N = \frac{F}{n} = \frac{\tau B}{n}$$

So the voltage SNR becomes,

$$SNR_v = \sqrt{\frac{B\tau}{n}}\,\frac{T_p}{T_{sys}} \qquad (1)$$

Showing sensitivity improves as the square root of the RF bandwidth and data collection time, degrades with the square root of the bin number, but responds directly to a reduction in the receiver system noise temperature.

Pulsar signal power is usually expressed in Janskys (J); the received source power corresponding to $1J = 10^{-26}$Watts/m^2/Hz.

The equivalent received power in terms of Boltzmann's constant and effective temperature is kT_JB Watts, where $k = 1.38.\ 10^{-23}$Watts/°K/Hz; T_J is measured in °K and again, *B* is the RF bandwidth in Hz.

Equating the powers in these expressions,

$$J\,A\,B\,.10^{-26} = 1.38\,.10^{-23} T_J\,B \text{ Watts, or, } J\,A = 1380 T_J$$

where A, is the receiver antenna effective collecting area (m^2).

Rearranging the equality,

$$T_J = J.A/1380\ °K$$

As an example, for a 30m dish with 60% aperture efficiency, the equivalent source temperature for a 1 Jansky pulsar source is, 0.31/2 = 0.154°K (1/2 factor for receiving a single polarisation).

The larger data collections in this project involved files of 1G samples and an RF bandwidth of 2MHz.

The system noise for the data collection telescope is stated as 110°K.

The temperature measurement uncertainty in each of n = 100 time bins within the pulsar period is therefore, dT = 110°K /√(10^9/100) = 0.035°K.

The signal-to-noise ratio per Jansky for the 30m dish is now predicted as,

$$SNR = 0.154/0.035 = 4.4/Jy.$$

Inspecting Figure 3 and, the plot baseline centre (~0.037373) is equivalent to the system temperature (110°K) and the scale is linear, we can calculate the Vela pulsar peak (0.03907) equates to 114.99°K. The source equivalent peak pulse power in Janskys appears to be, 4.99/0.154 = 32.4Janskys.

The baseline ripple is assumed zero mean and to have no effect on these calculations, but may account for some disagreement with published data. As a secondary check, the SNR measured from the data in Figure 3 is 99.24, using Equation 1, T_p is calculated as 3.45°K, or 22.4Janskys.

Base line level has been known to vary with the RTL SDR temperature, which should be closely controlled[4]; calibration tests have not always produced a consistent result.

Evaluation

Initially, 46 files relating to the Vela pulsar were collected in *rtl_sdr*, '.bin' files at sizes 100MB, 200MB, 400MB, 500MB, 800MB, 1000MB, and nominally 1600MB. The 1600MB files were truncated to just over 1GB due to the byte size limitation of integers in 'C' code derivatives**. Nevertheless the files produce were of excellent quality and more than sufficient for the present task. All data was collected in a 2MHz RF range within the Hydrogen line 1420MHz band using a RTL2832U DVB-T dongle tuned within a 150MHz IF band.

Figure 2 shows the Vela pulsar pulse power integrated over a 50 second 100MB file, combining some 560 pulsar pulses. The rotation period used with software *rapulsar.exe* to synchronise and integrate the data series of pulsar pulses was 89.3905ms.

** G Gancio has modified Osmocom tool 'rtl_sdr' (for linux –> rtl_sdr2) to overcome this limitation, allowing bin files to be recorded in excess of 30GB. Software developed in this project has also been modified to accept these larger files.

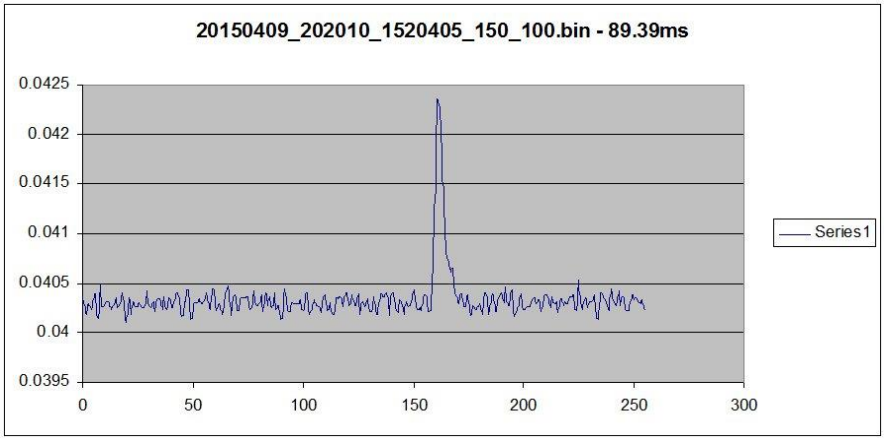

Figure 2 Synchronously Integrated Power, 50sec of Vela Pulses - 256 time bins

The software processing command line to produce this plot was,(see Software Appendix)

rapulsar 100.bin 100a.txt 2.0 256 89.3905

Using pulsar period values slightly either side of this figure broadens the response until the pulse is washed out and the base noise increases.

Integer multiples of this value inserts a corresponding number of pulses in the plot. When close to the correct period, but using twice or three times the expected period, plot symmetries can aid the period search task. Search time can also be shortened using *rapulsan.exe* on long files to reduce the amount of file data processed. Selecting a low (<100) number of time bins also helps period matching if power ripple or regular interference is present.

The period figure, found for the present data, exceeds recognised published values for Vela rotation[(2)], possibly attributable to the RTL SDR clock accuracy.

Figure 3 is the result of integrating a 1GB file of some 500seconds duration. Much improved signal-to-noise ratio is observed

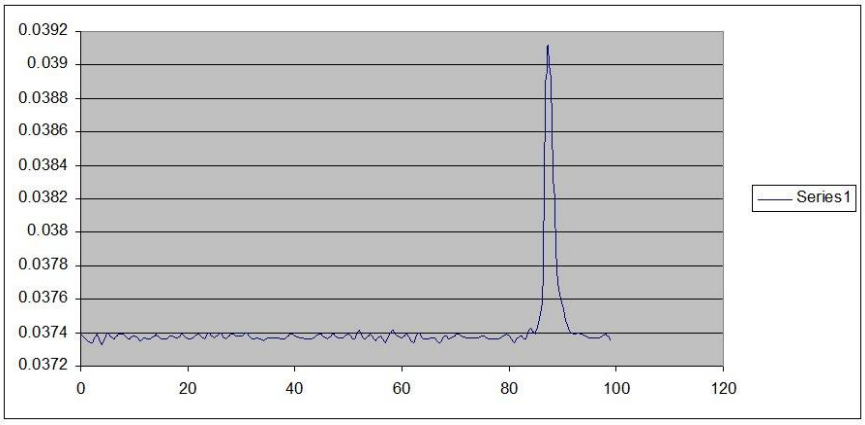

Figure 3 500sec Synchronous Power Integration - 100 time bins

Figure 4 depicts the same response except as an experiment, the pulse power data has been artificially reduced in the plot by a factor of 25 as might be expected from a dish of 6m diameter.

This pulse level is suggested as just sufficient for an amateur to do some reasonable work. Once an integrated pulse has been identified, there would be no problem in overcoming the RTL bin file 1GB limitation and stacking file results to obtain improved signal-to-noise ratio.

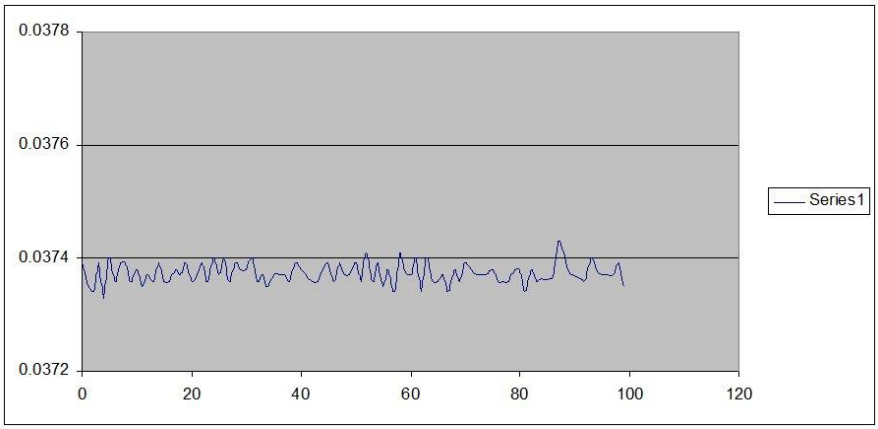

Figure 4 500sec Synchronous Integration (T_p/25; SNR ~ x4)

It is noted in Figure 2 that the baseline appears to exhibit some regular variation and this was shown to be caused by very low level, possibly power supply, ripple modulating the data. Figure 5 shows this feature using square-law detection software to show a short data time sequence.

In Figure 5, the red curve is the raw data using the *pdetect.exe* program and shows the unwanted ripple in the baseline clearly. *pdetect* simulates a square-law detector, in this case, set for a 1kHz video band width and performs this function by averaging the power in blocks of data numbering 1/video bandwidth, and outputting the results at the end of each block. The red amplitude plot is such that individual pulsar pulses are obscured. To assess the effect of the ripple not being present, a sine wave of the same frequency and phase (blue) is simulated and subtracted from the raw data to produce the lower black plot.

This still contains unwanted noise but individual pulses can now be observed, for clarity, aligned to the negative peaks of the magenta sine wave, which has been adjusted for the pulsar rotation period of 89.39ms.

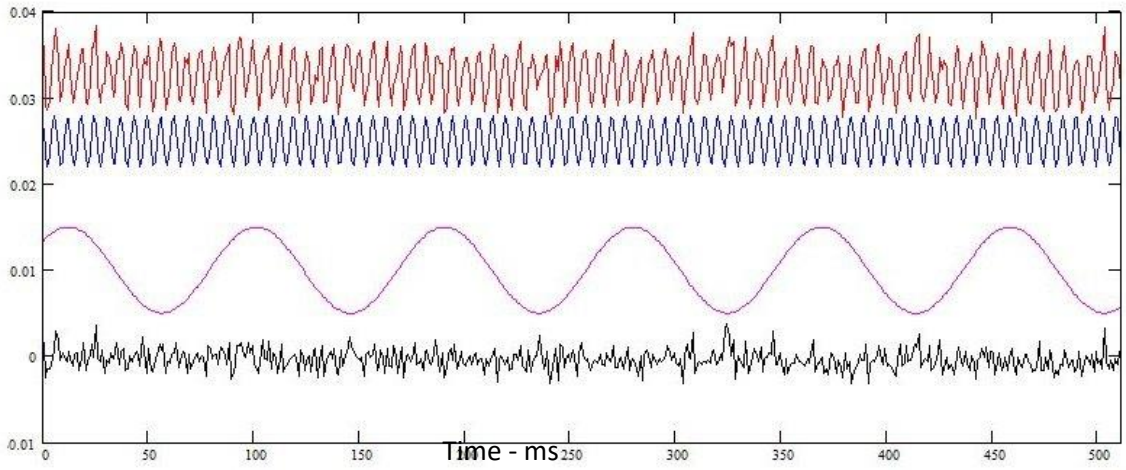

Figure 5 Time-base Plot of a Typical Data File

Determining Pulsar Rotation Rate

In principle, the pulsar rotation period and rate can be determined from the timebase plot, using the *pdetect* program by identifying pulsar pulses and measuring the pulse arrival times. Most pulsars are not so powerful however and may not be visible, but spectral integration using long or multiple averaged FFTs can recover the rate information.

The pulsar signal is effectively pulse modulated wideband noise and indistinguishable from the receiver system noise. The detection process demodulates this to a DC pulse train repeating at the pulsar rotation period, plus video noise. The resulting pulse train FFT spectrum comprises a number of spectral lines spaced at 1/(pulsar period) together with broadband system and pulsar video noise spread over the FFT spectral range. Detection of the system noise also produces a constant DC component in all FFT bins.

The signal-to-noise ratio of pulsar components can be improved in either of two ways; one by increasing the FFT length and the second by averaging multiple shorter FFTs. Both methods are equally effective in improving the SNR; longer FFTs giving better resolution. FFT averaging is feasible over many processed data records to get sufficient integration for weak pulsar signals.

Best period accuracy is assured using the frequency of the highest identified period harmonic.

If 'k_n' is the pulsar FFT data n^{th} harmonic bin number, the pulsar rotation rate is given by,

$$R_p = k_n B_v/(nP) \text{ or the period } T_p = nP/\ k_n B_v.$$

where, 'B_v' is the video band specified in the *pdetect* command line and 'P' is the number of FFT points/bins.

The real data FFT spectrum plot covers the frequency range 0 to $B_v/2$ with a frequency interval/bin of B_v/P; the best choice of these parameters depends on the pulsar rotation rate and timing accuracy expected. Ideally there should be several video samples ($1/B_v$) within the pulsar pulse and the number of FFT bins P should be large enough so that the first pulsar spectral line (at $P/T_p\ B_v$) is far enough away from zero to be clearly visible.

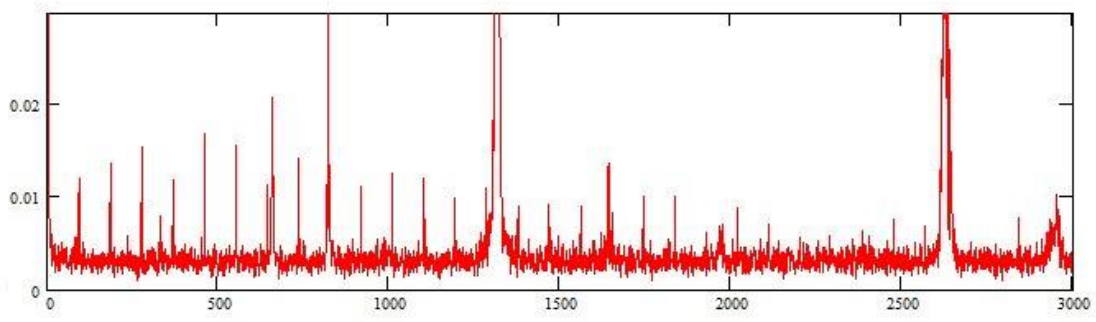

Figure 6 Average of 4 x 8192-point FFTs

Figure 6 shows the average data of 4 consecutive 8192-point FFTs derived from 1kHz bandwidth *pdetect* data (from *rtl_sdr* IQ sample pairs at 2MHz rate), the pulsar rotation rate harmonic spurs are clearly evident, as are some large interference components (around bin 1326 and 2652, equivalent to ~ 162 and 324Hz).

The 31st harmonic lies in bin number 2841. The Vela pulsar rate and period are then derived as described above; period = 31 x 8192/2841 = 89.388244ms – very close to the value found experimentally using *rapulsar* program.

The result using all the data in a single 131,072-point FFT is 31 x 131072/45455 = 89.39021ms.

The program *pafft.exe* enables the various key parameters to be chosen and outputs a text file for Excel to produce a spectrum display similar to Figure 6. The parameters can be varied to optimise the presentation and aid the estimation of the pulsar rotation rate/period.

Conclusions

Useful data has been collected on the powerful Vela pulsar with a 30m dish facility using an RTL2832U SDR dongle. Simple integration software based on a known/derived test value of the pulsar period has shown to effectively improve the pulse to system noise ratio so that pulse detail can be observed.

For the observed conditions and resulting signal to noise ratio, a reasonable estimate can be made of the minimum useful antenna aperture for amateurs to effect detection. For the Vela pulsar this aperture estimate, from the process leading to Figure 4, is 6m.

Bearing in mind that the Vela pulsar is probably the most powerful that has been discovered (maybe not as strong as calculated here) and most pulsar powers are much less than 1 Jansky, opportunities for amateur radio astronomers appear limited.

Synchronous pulsar pulse integration is effective and can be extended to several hours if necessary. Enabling software includes developments to accommodate much larger files or to collate many short (1GB) sections.

Other routes to improving pulsar detection with smaller dish sizes are to reduce the system noise temperature, the use of a wider RF bandwidth SDR/bank of RTL SDRs, or alternatively moving a lower RF band.

For Vela, an improved 50°K system temperature (x2.2) coupled with a 10MHz RF bandwidth SDR (x√5) or 5 suitably tuned 2MHz RTL SDRs*** together with processing 30GB data files (x√30) would enable a 2.2x√5x√30 antenna area reduction This brings the dish diameter required to about 5.8m to match the performance to the present 30m dish system. A 3.5m aperture with these improvements could achieve an SNR of 36 compared to 99 in Figure 3. 30GB (~4 hours) need not be collected in one session but the sensitivity can be recovered from an equal set of smaller files. Smaller files must be sufficient to identify and correct the pulse phase so that re-alignment and synchronous adding/averaging can be performed.

PSR B0329+54 is the strongest pulsar in the northern hemisphere and is logged at about 1/5 of the power of the Vela pulsar but should still be detectable with an optimised 3.5m dish system. This may still be within many amateur radio astronomer's capability, especially if prepared to combine several 30G observations.

Wider band SDRs (RASDR or Airspy) and lower frequencies may require de-dispersion pre-processing.

Finally, longer term tracking and integration, reduced system temperature, reduced interference, lower frequencies, de-dispersion and wider SDR bandwidth coupled to an antenna of 3.5m upwards seems to offer the amateur a way ahead.

Postscript

This has been very much a project undertaken with minimal pulsar experience. However, pulsar data recorded using a cheap RTL DVB-T dongle has responded to some fairly basic signal processing algorithms although some results are at variance with published data. With design care plus a tracking 3.5m dish system, it seems feasible for amateurs to detect and analyse the stronger pulsars. For the future, there are a number of areas that could be explored for the further development, including,

1. De-dispersion, by coarse FFT channelling and post integration combination.

2. Filtering interference, or,

3. Pulsar rate FFT spur filtering + inverse FFT prior to synchronous integration.

4. Multiple SDR injected-noise timing management with RasPi back-end processing+.

5. Investigate amateur use of Tempo2.

May many others get the thrill from seeing a pulsar pulse shape appear out of noise as the rotation period is adjusted to the perfect value.

*** Stability of multiple RTL SDRs can be much improved with air cooling[4]. Uncooled, the tuned rf frequency and gain can drift significantly during operation.

+ see Appendix 3

References

1. http://www.iar.unlp.edu.ar/index.html

2. http://www.atnf.csiro.au/research/pulsar/psrcat/

3. http://zmtt.bao.ac.cn/pulsar_cof_beijing/afternoon_509/mkeith_search.pdf

4. http://www.y1pwe.co.uk/RAProgs/FrequencyStabilityU2.doc

5. http://iopscience.iop.org/0004-637X/498/1/365/fulltext/

Appendix 1. - Software[****]

***rapulsar2.exe* - Synchronous Integration**

This software processes RTL .bin data collected with an RTL SDR receiver system.

It integrates the IQ power data synchronously on a timebase adjusted to or very near to the pulsar period. The result is a text file that can be viewed with Excel or mathcad programs showing the integrated pulse power shape at some arbitrary phase dependant on the initial file timing conditions.

A typical command line is....

rapulsar2 <datfile.bin> <outfile.txt> < RTL data rate (MHz)> <No. data points> <Pulsar period (ms)>

For large files when adjusting the pulsar period, a smaller subset can be inspected using the modified program....

rapulsan2 <datfile.bin> <outfile.txt> < RTL data rate (MHz)> <No. data points> <Pulsar period (ms)> <File divisor>

The file divisor integer shortens the processed file to the file divisor factor.

***pdetect2.exe* - Square-law Detector**

This software processes RTL .bin data collected with an RTL SDR receiver system.

It acts as a software, square-law detector. The result is a text file that can be viewed with Excel or mathcad programs showing the video integrated detected power - time response. It integrates data in blocks proportional to the inverse of the video band figure and outputs the block result.

A typical command line is....

pdetect2 <datfile.bin> <outfile.txt> < RTL data rate (MHz)> <Video Band (kHz)>

[****] Latest versions can now process .bin files much larger than 2GB, identified with the post nominal '2'.

<File divisor>

As before, the file divisor integer shortens the processed file to the file divisor factor.

***pafft2.exe* - Pulsar Rotation Spectrum**

This software processes RTL .bin data collected with an RTL SDR receiver system.

It calculates and averages FFT spectra formed from square-law detected data as specified in the command line. The result is a text file that can be viewed with Excel or mathcad programs showing the pulsar pulse spectrum, from which rotation rate harmonics may be identified and the rotation rate/period can be calculated.

The period information can then be input to *rapulsar* to seed accurate timing estimation.

A typical command line is….

pafft2 <datfile.bin> <outfile.txt> < RTL data rate (MHz)> <Video Band (kHz)>

<FFT size>

Software Link

http://www.y1pwe.co.uk/RAProgs/NewSW2.zip

Appendix 2. Pulsar J0437- 4714 Experiment

This appendix summarises RTL SDR results for a weaker, faster rotation rate pulsar - J0437-4714 using the software developed for this project.

Note that the pulsar spectral lines are very small compared to the interfering signal level and requires 1GB files and expected harmonic component relations to identify them.

Techniques to accumulate harmonic components have been described[see Reference 3].

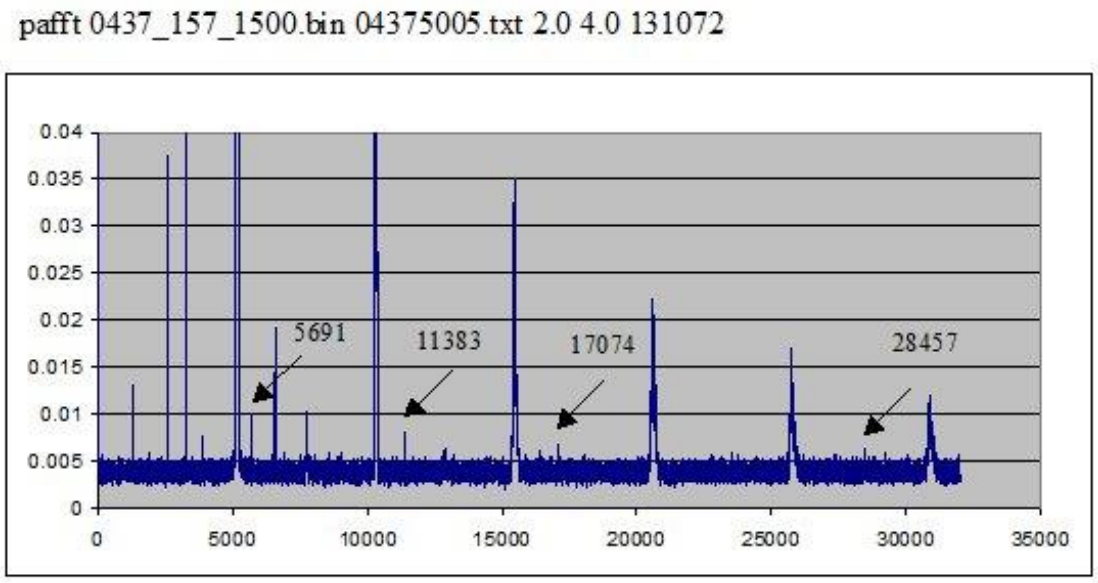

Figure A1 Detected Power Spectrum - J0437-4714

Calculated rotation period, T_{fft} = 131072 x 5/28457/4.0 = 5.75746ms.

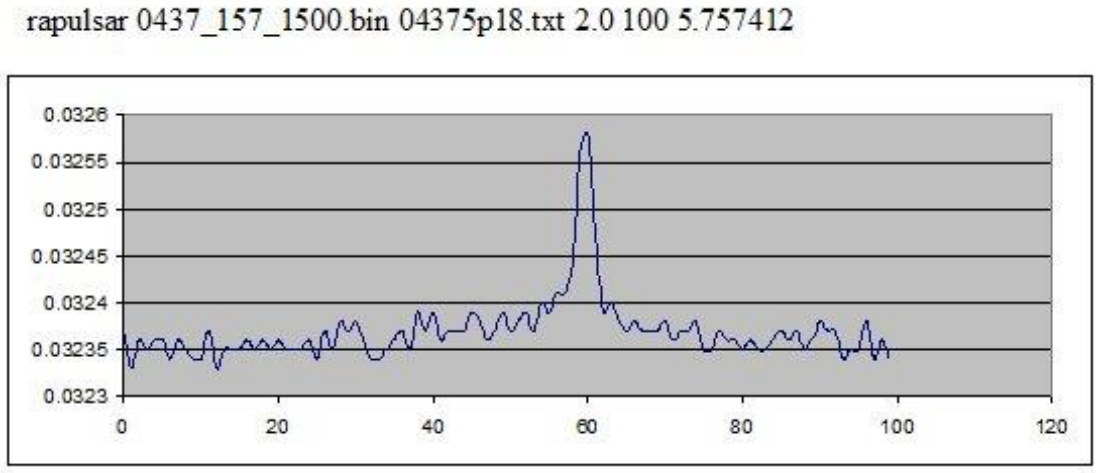

Figure A2 Synchronous Integration - J0437-4714

Optimum period result by trial and error, T_{trial} = 5.757412ms. SNR_v ~x20.

From Figure A2, pulsar peak temperature = 110° x0.03258/0.3235 = 0.78°K, o r ~ 5.06Jy. This compares favourably to the peak average expected of 5.6Jy from Reference (5),

Radio Pulse Properties of the Millisecond Pulsar PSR J0437-4715. I. Observations at 20 Centimeters., Jenet, FA, et al., 1998.

Appendix 3 - Quad RTL SDR Pulsar receiver

Introduction

Multiple RTL SDR's locked by a single master crystal oscillator and ambient air cooled are an economical approach for multi-baseline interferometry and high sensitivity wide-band pulsar detection receivers. Figure A3 shows a 4-channel digital receiver block diagram producing complex data files driven and collected by Raspberry Pi mini-computers. For interferometry, the SDR's are tuned to the same frequency and calibrated to phase track. For Pulsars or wide band operation, the SDR's are tuned to adjacent bands. Calibration and synchronism of data files is similar in both applications. The receiver cost, less the controlling PC, is around £300.

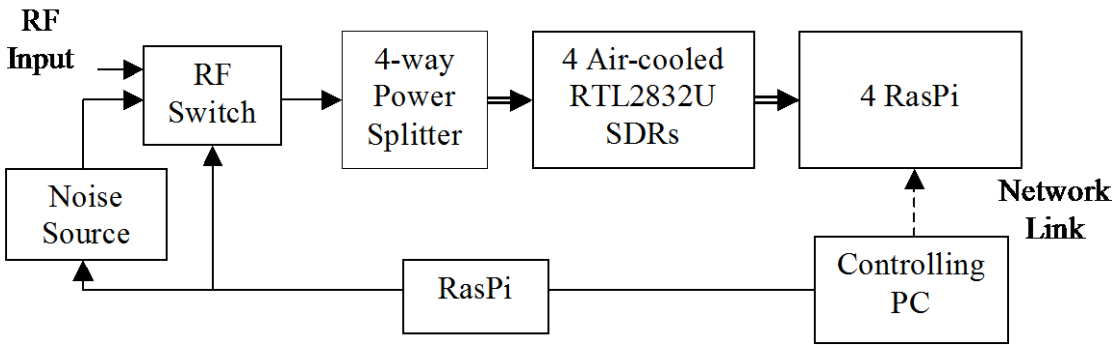

Figure A3 10MHz Bandwidth 4xSDR Digital Receiver

Hardware Notes

1. RF switch - 1-pole, 2-way, electromechanical (ms switch speed) or PIN (us switch speed). The latter type may be best for more accurate file offset correlation (Mini-Circuits, ZMSW-1211 is suitable ~£60).

2. Noise source - (ebay SMA noise tracking source ~ £15).

3. Power splitters - three 2-way or one 4-way RF power divider.

4. Bare RTL2832U's with mini heatsinks on all ICs, run from a single temperature compensated crystal at 28.8MHz, all mounted in an air-cooled metal box[4].

5. 4xRasPi with 64GB USB memory.

Operation

PuTTY[a] on the controlling PC manages operations on all RasPi's via SSH[b]. Programs are run in RasPi terminals via the controlling PC. *rn_rtlat2* runs the Osmocom *rtl_sdr* data acquisition program at a set time to nearly synchronise all 4 SDR data collection.

The delay between start command and the program run time may vary due to the processor housekeeping, clock requests and clock accuracy. Delays are unpredictable but limited to few or low tens of milliseconds.

On completion of data recording, data files are downloaded to the controlling PC for final processing. Accurate synchronism can be achieved by switching on and off a noise signal and using correlation software to identify offsets required to synchronise SDR data files. Synchronism accuracy for pulsars only need to be a fraction of the pulse dwell whereas alignment within a clock cycle is necessary for interferometry to limit phase offset which can be achieved by noise amplitude correlation.

Operation Sequence - Pulsars

Data collection

1. Set switch to select noise source.

2. Start 4 SDR's recording using *rn_rtlat2* at programmed time, 4 SDR's with set data rate at 2.5MHz to cover 10MHz band.

3. Turn on noise using 5th RasPi with *rn_prgat.*

4. Random on-off noise modulation for 1sec to simplify correlation.

5. Switch to signal path for data recording.

Data correlation, Matching

1. Select SDR1 data file as master.

2. Run *cor_tim2* on 1+2, 1+3 and 1+4 data files, note noise source timing.

3. Determine file offsets for correlated alignment.

4. Calculate de-dispersion times and adjust offsets.

5. Run *f_align2* on all 4 files to match start positions and file lengths.

---

[a] http://www.putty.org/

[b] apt-get install openssh-server openssh-client

6. Run *pafft2* on the four data files, average spectrum data and inspect for rotation spurs.

7. Run *rapulsan2* on files to for synchronous integration of pulsar pulse shape.

Conclusions

The architecture and processes described offer an economical approach to broad-banding and time calibrating a pulsar receiver to improve system sensitivity and also provide a simple and convenient method of de-dispersion.

The method is suitable for extending the frequency band and provides raw data files that can be investigated at leisure.

Data files of particular sources can be collected on multiple occasions and the results added and combined to further increase the receiver effective sensitivity.

PW East, GM Gancio. May 2015

Editor's Note: The following paper was originally translated into English, so I have made a few minor edits to the grammar. I also converted it from a PowerPoint style, both at the request of the author. I hope the conversion does not cause the reader confusion

RADIO ASTRONOMY

SOLAR ECLIPSE on 20 March 2015

Radio observations, analysis and results

By Jean-Jacques MAINTOUX –F1EHN / F6KSX –AAV

In collaboration Joachim DF3GJ / DL0SHF

Last update: 30 April 2015

Solar Eclipse on 20 March 2015Observation, analysis and results

F6KSX –AAV radio astronomy station (radio telescope)

- Expected performances
- Forecast of the solar eclipse
- Measurements -Analysis and results
- Simulation -Analysis and results
- Conclusions
- References

F6KSX –AAV Station –Radio telescope

- Parabolic dish antenna : 3.3m diameter –Vertical Linear Polarization
- Frequency band : 21cm (dedicated to radio astronomy)
- System Noise Temperature : 60 K
- Digital receiver on IF 60 MHz / Bw=2,5 MHz(sample frequency)
- Real-time display with FunCube device and Spectravue

- GPS –Date and Frequency reference
- Data recording and automatic tracking
- Local Oscillator for 21cm receiver
- Tracking interface for positioning syste
- Real time display and signal post-proce

Expected performances

SoitT = Temperature, k = Boltzmann cst, cs => cold sky, sun => sun, sys => system, F = 1420 MHz, Wavelength λ = c/F => λ = 0.211m, Aeff = effective Area, Bw = Bandwidth, Tant=> Antenna temperature, Tsys=> System temperature

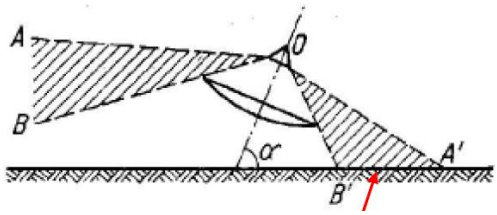

- 21cm STATION :
  - Antenna @21cm
    - D=3.3m, Gain = 31dBi => G=1260
    - Aeff= G*l²/4pi = 4,46m²
    - Diagram aperture = 4.4° (half power beamwidth - HPBW)
    - Tant_cs = 15K (Tsky ~ 5K, Tlobes = 10K + spill over estimated from measurement)
  - Receiver
    - Lr= antenna to receiver losses = 0,1 dB => Lr = 1,023
    - Receiver Noise temperature: Tr = 34K (NF = 0.48 dB)
    - Bw = 2.5 MHz (to enhance measurement resolution)
  - System temperature
    - Tsys_cs = Tant_cs + (Lr-1)*290K + LrTr (beamed on cold sky @ ~ 5K)
      - Tsys_cs = 57 K (cs = Cold sky / near galactic poles)
  - Frequency : 1422 MHz (Outside H1 line radiating)
    - Here we are interested in the thermal radiation from the Sun (ionized gas at high temperature and black body radiation type
    - Radio radiation is a tiny part of the solar radiation mostly centred between infra-red and ultraviolet.
    - http://en.wikipedia.org/wiki/Sunlight
  - Sun flux radiation
    - Flux @ 1415 MHz : 85 sfu
      - From San Vito observatory (or 85 10-22W/m²/Hz)
  - Expected signal level (solar excess noise)
    - Tant_sun = Flux * Aeff / (2*k) = 1374K (for one polarisation)
    - Received signal measurement is similar to (S+N)/N with :
      - S = k * Tant_sun* Bw
      - N = k * Tsys_cs* Bw
      - Solar excess noise = (Tant_sun / Tsys_cs) + 1 = 25, or Y = 25 ou 14 dB

Both measurements done with the same bandwidth => Bw= 2,5 MHz

This ratio is commonly named Y factor. Here, the ratio is coming from 2 measurements consecutively with beaming to a cold sky area and then to the sun (before and after the eclipse).

Solar Eclipse forecast

Near Paris, this eclipse was partial with cloudy weather not permitting any optical observation. Monitoring was carried out via Internet (Pic du Midi). The recordings were started at 08:19:00 UTC. To our surprise the eclipse radio event started contrary to predictions (see results). The elevation of the Sun was 22° at an azimuth of 118°.

The maximum has either not been marked (see results). The recordings were stopped at the end of the eclipse around 11:00 UTC. The elevation of the Sun was near 40° for an azimuth of 160°.

Visibility of the eclipse

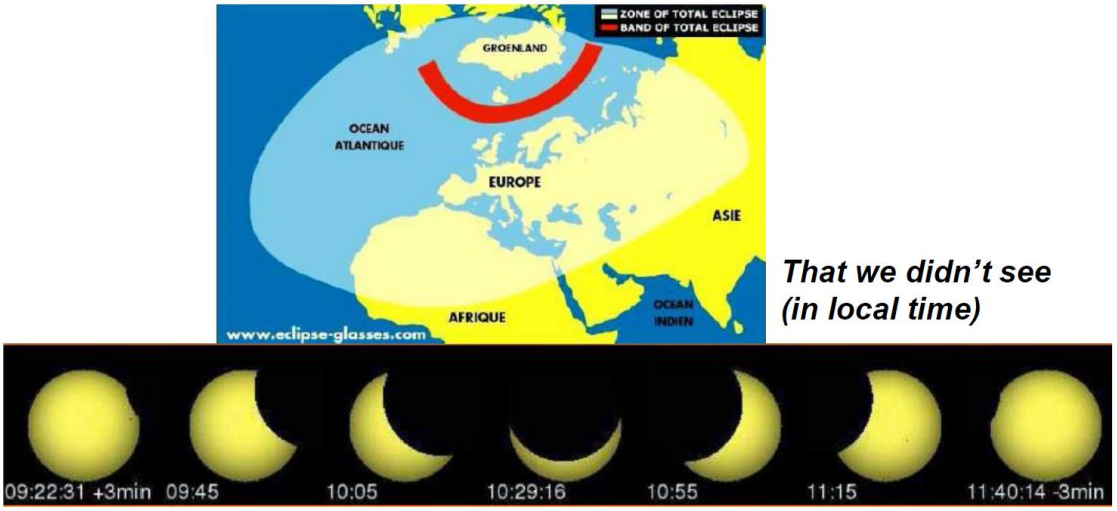

Raw measurement

During the eclipse, the solar flux is intercepted by the moon. Here, the temperature of the Moon is negligible (angular size low compared to the antenna aperture and still present in the lobe)

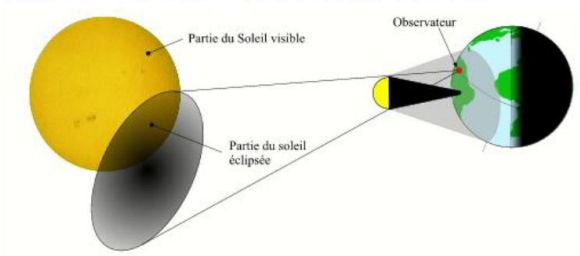

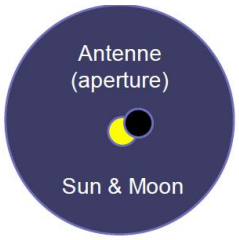

With automatic tracking of the sun position

Raw Y factor (en dB)

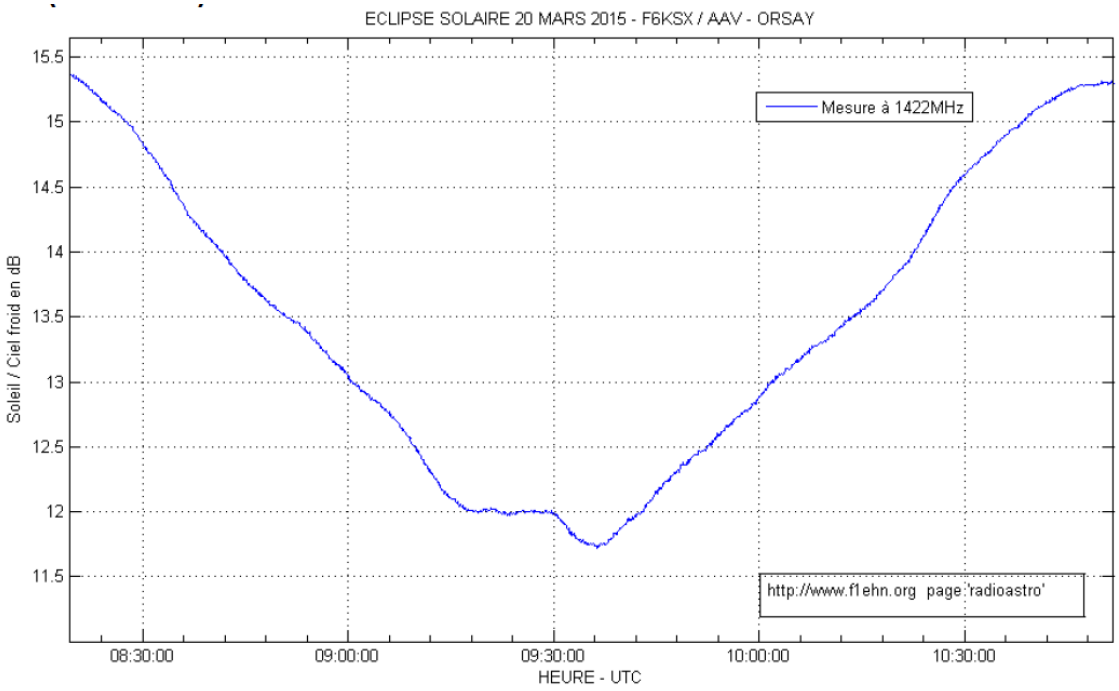

Analysis

- System Noise Temperature (Tsys)
  - The eclipse began at low elevation. The system noise temperature is then higher, this increase is mainly linked to the side lobes of the antennae pointing towards the ground, trees and surrounding homes.
  - The figure below shows the system temperature depending on the elevation. The raw measurement will be corrected by taking into account the reference level measured on the 'Cold Sky' away from the Sun.
  - The lower sensitivity meant higher Tsys, is then compensated.

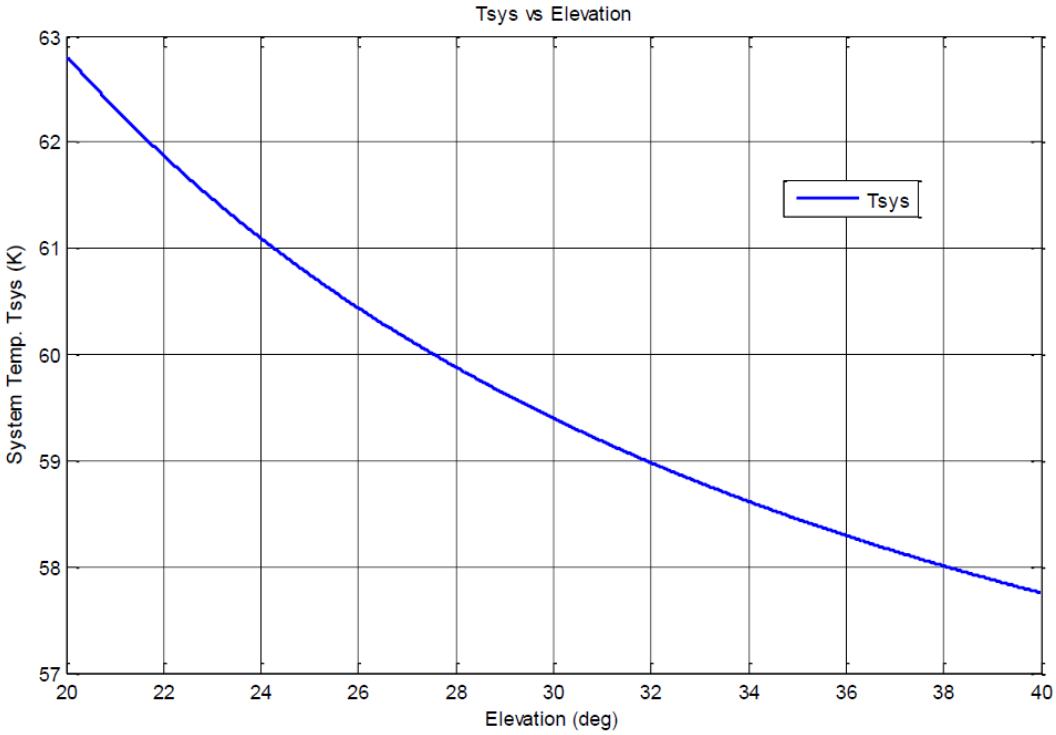

Results and comments

The curve below shows the antenna temperature deduced from the Y factor and system temperature by reversing the formula's prediction of the factor Y. It shows the variation of the solar flux received during the eclipse.

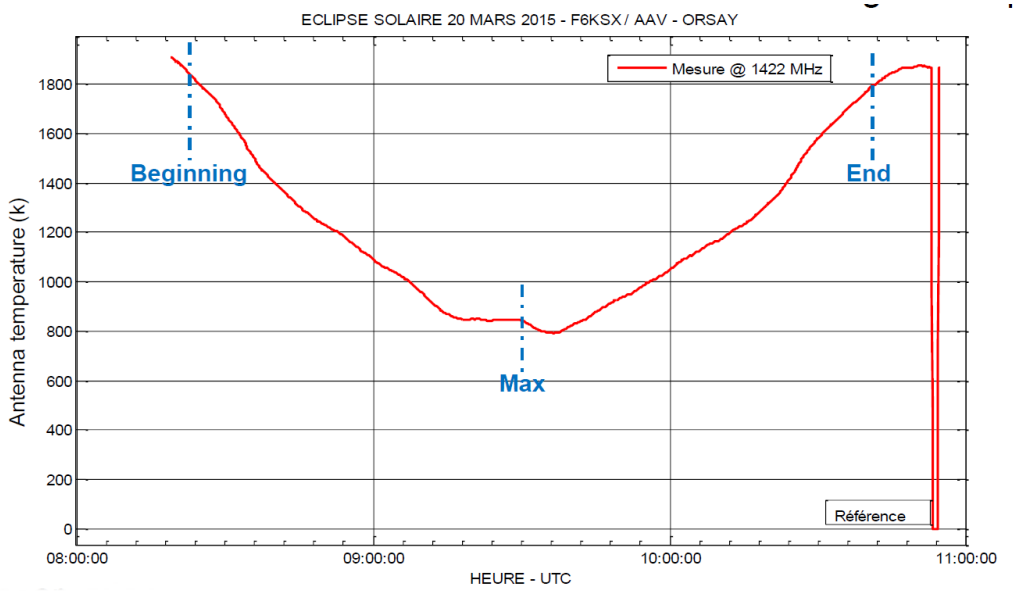

First observations: The radio eclipse is wider than the optical eclipse. The maximum of the eclipse (the curve minimum) is shallower than expected (57% compared to 79% for obscuration). The antenna temperature is higher than expected, the curve is not uniform and has numerous kinks on its flanks.

Results and comments

The radio eclipse is longer and less "deep" than the optical eclipse. Indeed the sun at 21 cm can be considered to be "larger". The Corona extends far beyond its visible diameter and it radiates the most important flux at this frequency. The obscuration is less deep because the Moon cannot completely overshadow the solar corona.
The curve below shows 3 simulations, for optical, with a larger Sun and then with "annular" corona and compared to the flux measurement (obscuration in dB).

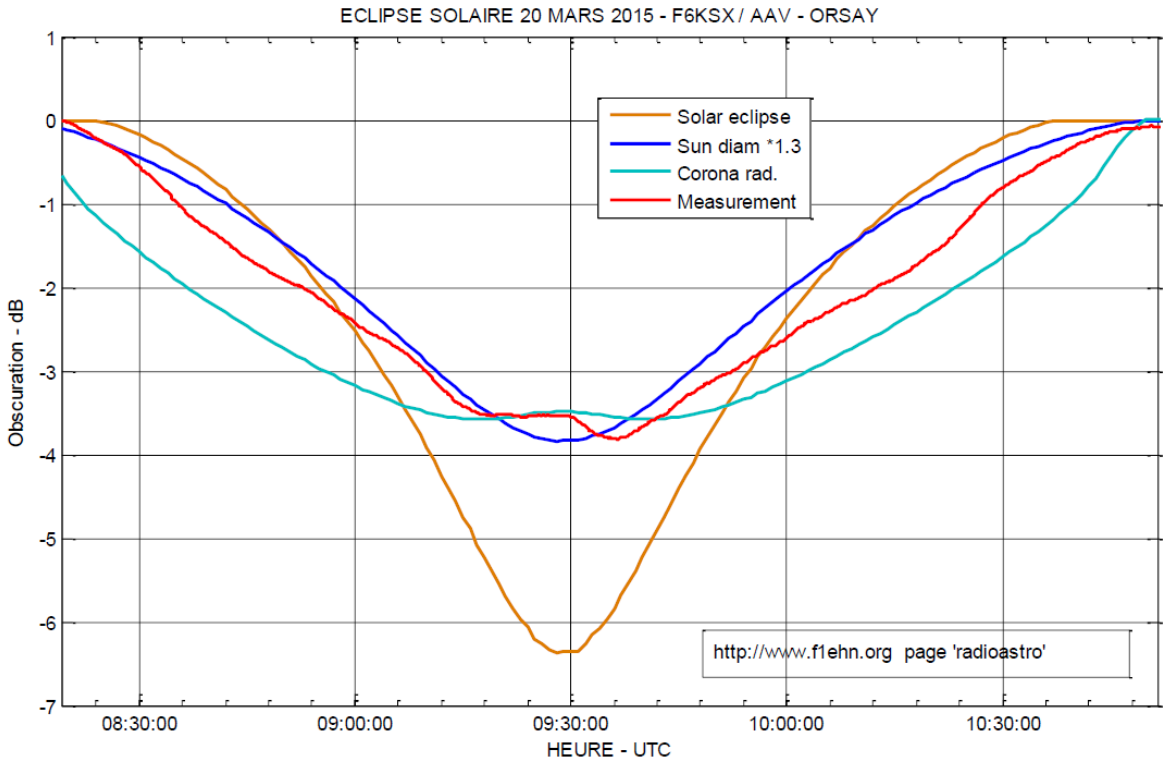

It can be seen that none of the three simulations are consistent with observation. The observation lies between the annular radiation (here it is too pronounced) and a larger diameter solar radiation.
More observation presents an asymmetry at the time of the maximum as well as deformations in its flanks.

The antenna temperature is higher than expected, and the curve is not uniform and has numerous kinks on its flanks. The origin may be caused by: the presence of radiating sources, themselves eclipsed at certain moments by the Moon (see simulation) and the temperature rise.

The curves below shows the Y factor in dB referenced to its maximum value. This curve allows us to identify different observed deformations and compares the results to those of the DL0SHF station and DF3GJ analysis.

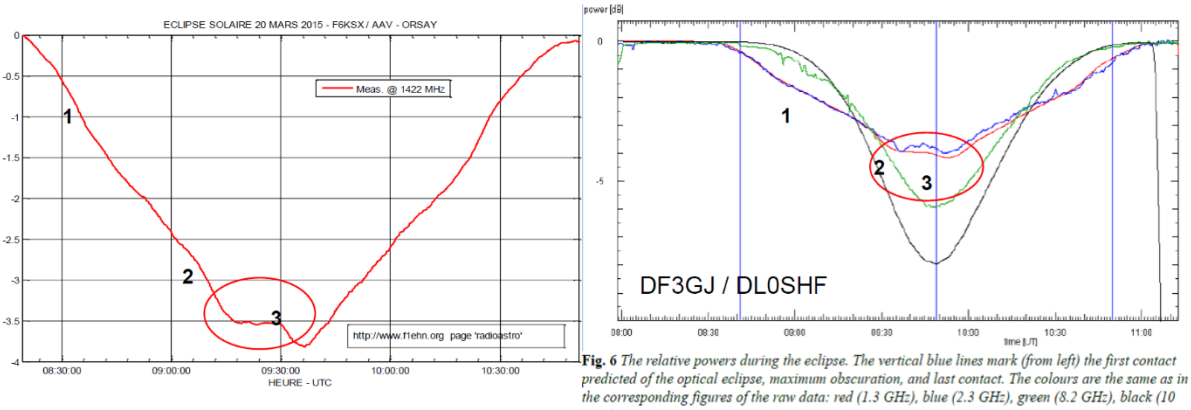

Fig. 6 *The relative powers during the eclipse. The vertical blue lines mark (from left) the first contact predicted of the optical eclipse, maximum obscuration, and last contact. The colours are the same as in the corresponding figures of the raw data: red (1.3 GHz), blue (2.3 GHz), green (8.2 GHz), black (10 GHz).*

It appears that the 2 stations, despite their distance and maximum being shifted, show the same phenomenon. This result is therefore not coming from a bad measurement or a local phenomenon. The observation is therefore correct. Marks 1 to 3 will be used later to identify these moments of the eclipse.

Simulations

The measurements are intermediate between the simulation made with a larger diameter Sun and model considering radiation of the outer corona represented by a ring. The actual model is more complex (see Reference Coutrez) and the Sun is very active and its behaviour is complex. Subsequently, the simulation takes into account an external diameter of the corona equal to 1.2 times the nominal diameter. The thermal radiation from the Sun is also taken into account.

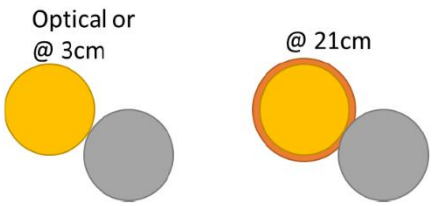

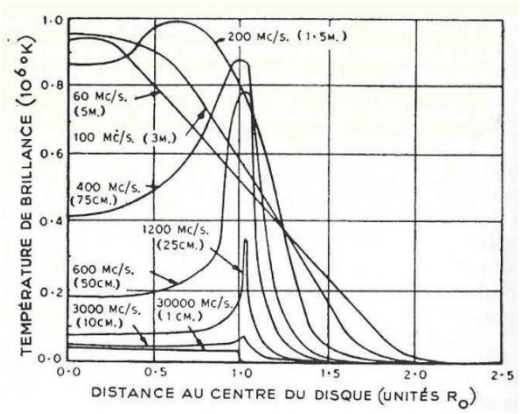

Observations

Other kinds of observations are considered in order to support the conclusion of the presence of several additional radiating sources. Thanks to BASS2000 database, Climso Halfa videos are used to reveal burst areas corresponding to the marks 1 to 3

Close-up of Mark 2

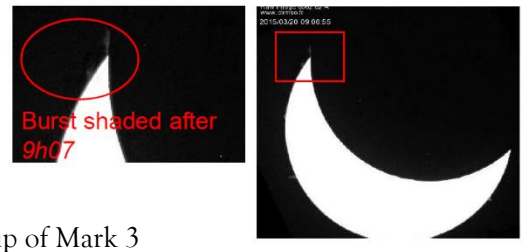

Close-up of Mark 3

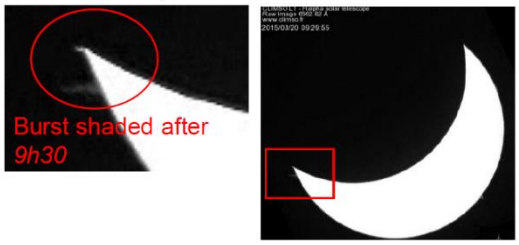

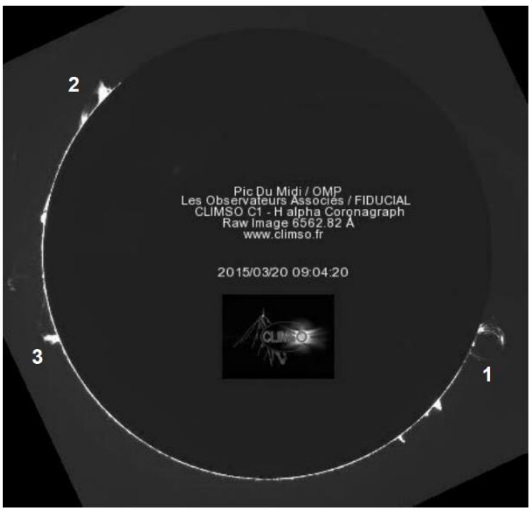

Other observations are considered in order to support the conclusion of the presence of several additional radiating sources. The RATAN-600 radio telescope is used to reveal the Sun in radio. It provides surveys between 3 and 24 GHZ (10 to 1.25 cm). The image below is extracted from the eclipse observation supplied by RATAN-600. The eclipse being less pronounced at that location, gives additional information on the position of the sources. For example, “1” isn’t shaded but “2” is totally shaded during the eclipse. See reference.

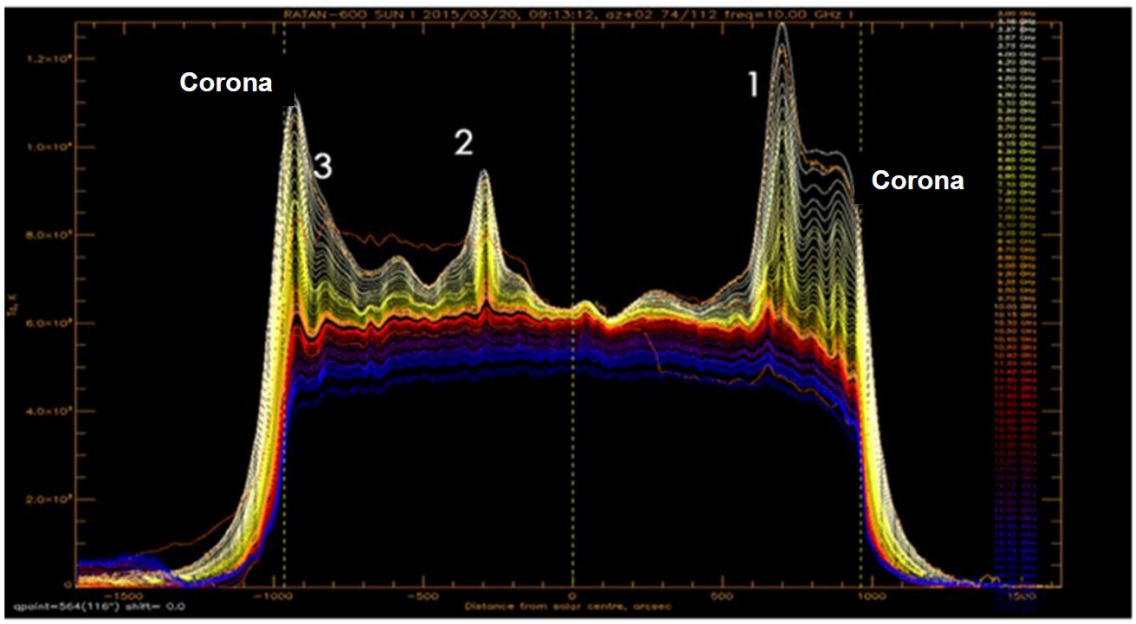

Simulations

The analysis of observations has taken a lot time and the main findings are presented. From this analysis, simulations with 1, 2 or 3 radiating sources were performed. The surface of the Sun is very complex, there should be more radiating sources. We should also use more accurate models, therefore the simulations were limited to 3 radiating sources.

The figure below shows the progress of the eclipse and the position of the 3 sources considered.

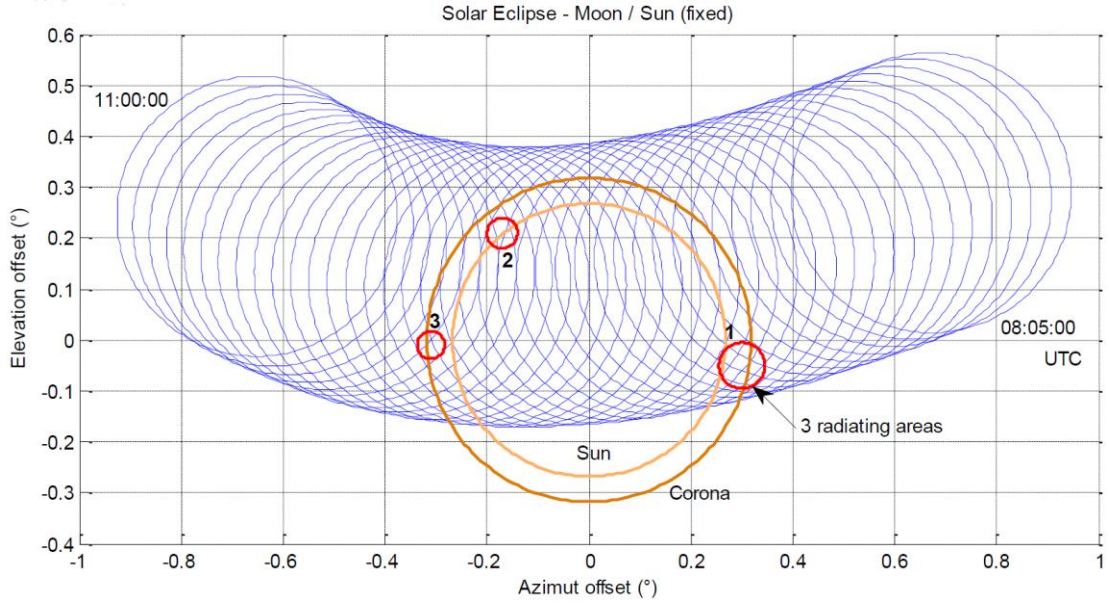

The simulation is broken down into different contributors. The figure below shows the contribution of each element to the simulation presented on the previous page.

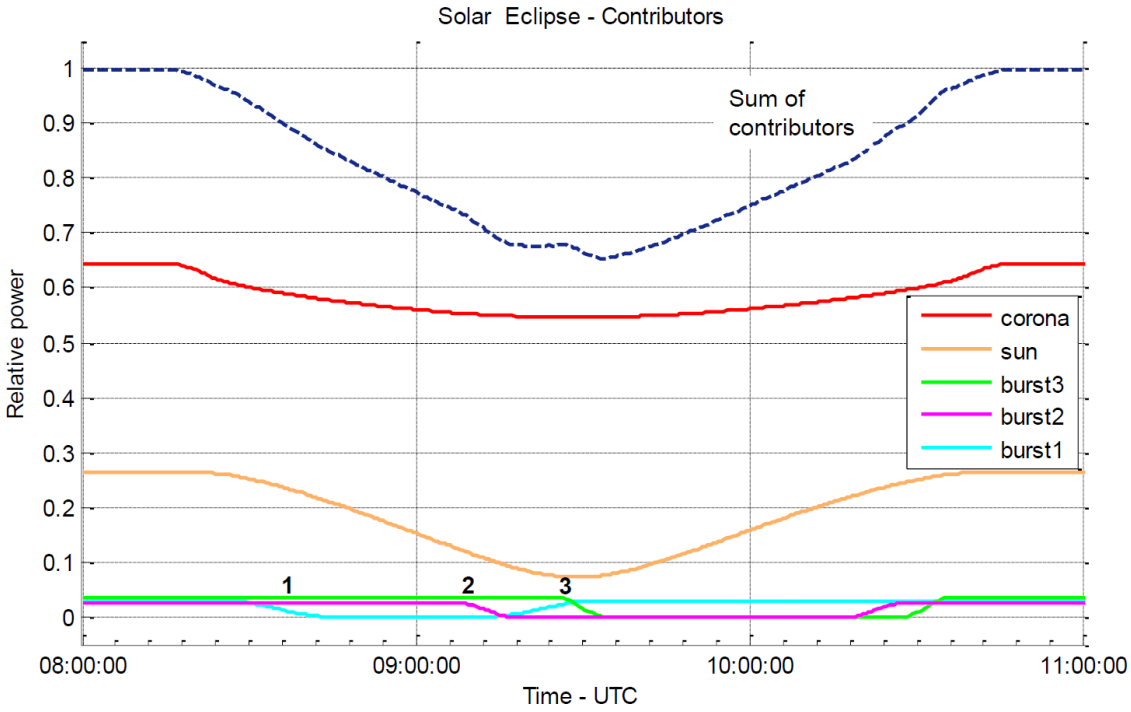

Simulations involving 1, 2 or 3 sources were made. 3 sources gives the following result. The number of parameters is important (temperature, position and dimensions of the radiating sources, dimensions of the corona, the coronal and solar temperature) they are detailed at the end of this presentation.

The figure below compares the result of simulation to the measurement.

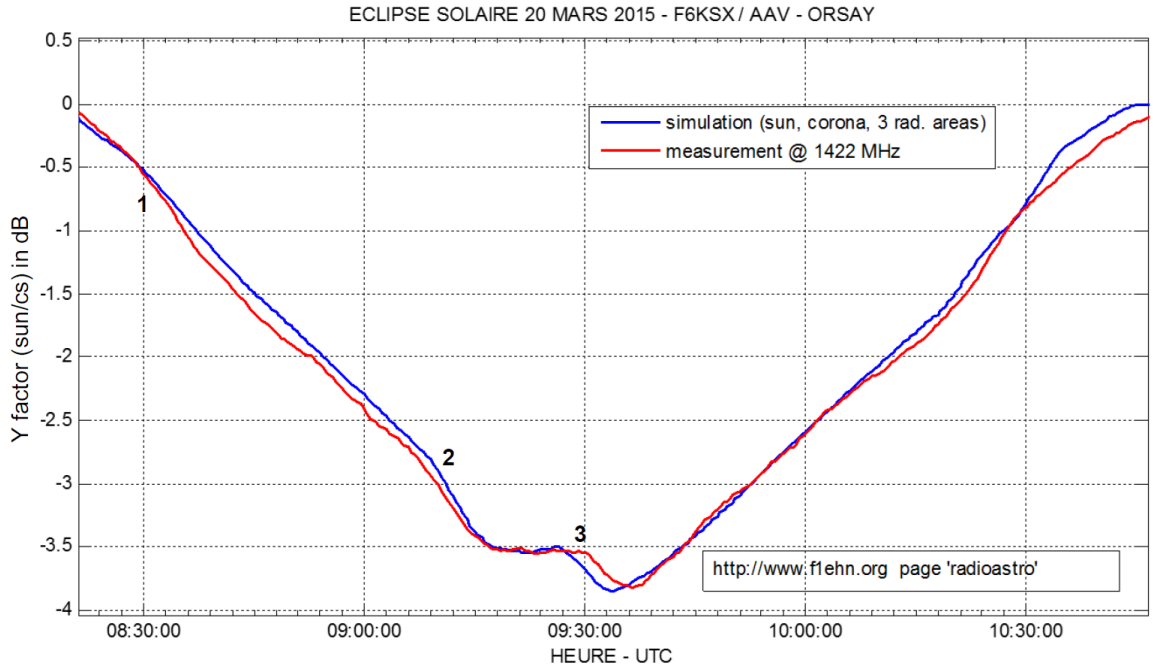

Conclusions

Originally, during the preparations, the measurements seemed relatively simple and easy to understand. From the 1st moment of measurement, it was the opposite. The eclipse began earlier, the curve was not simple, the maximum was not on time and the received signal was stronger than expected.

We obtained a complex observation which reflects the complexity of the Sun.

The analysis made possible by other observations, those of Joachim DF3GJ (DL0SHF) have allowed a better understanding of the phenomenon observed. We were thus all able to develop reports leading to very similar conclusions.

The simulations are designed to explain the observation made but they cannot be considered as a final and accurate result. For this, it would require more information and observations. The Sun is a very active and the radiating areas may be more numerous, of different shapes and evolve over the duration of long time observation for certain phenomena (like bursts).

For some stations, having a narrower antenna aperture changes could occur during observation (radiating sources close to the outskirt of the Sun) and therefore the results may be different.

Different materials or elements used are referenced (see following pages).

Unfortunately, it will be difficult to reproduce such experience in the future as it would require relocation of the telescope to another country. However, this shows that the observation of the sun always brings new surprises and continuous, stable and well calibrated observations must be carried out, as well as plenty of time for analysis to reveal all this complexity. This is the difficulty of radio astronomy.

Thanks to the AAV members who participated in this experience as well as J-P F1OI and OBSPM contacts for different exchanges.

References

- Sun –Wikipedia : http://en.wikipedia.org/wiki/Sun
- Joachim Köppen DF3GJ / DL0SHF
  - Simulation tool : http://sat-sh.lernnetz.de/applets/RadioEclipse/index.html
  - DL0SHF : http://sat-sh.lernnetz.de/indexEE.html
  - Observation : http://sat-sh.lernnetz.de/pdf/Eclipse2015.pdf
  - Analyses : http://sat-sh.lernnetz.de/pdf/EclipseAnalysis.pdf
- CLIMSO :
  - Solar imagery
  - http://climso.fr/en/
- Observatoire de Paris (OBSPM)
  - DatabaseBASS2000
  - http://bass2000.obspm.fr/home.php
  - video
    - ftp://ftpbass2000.obspm.fr/pub/climso/film/1503/imoa_video_512_00C1_20150320.mpg
    - ftp://ftpbass2000.obspm.fr/pub/climso/film/1503/imoa_video_512_00L1_20150320.mpg
- RATAN-600
  - http://www.sao.ru/Doc-en/SciNews/2015/eclipse2015/
  - http://www.sao.ru/
- Tracking(Automatic tracking and Planner for simulation forecast)
  - EME System
  - http://www.f1ehn.org
- Coutrez–"Radioastronomie"
  - Solar brightness temperature over different frequencies

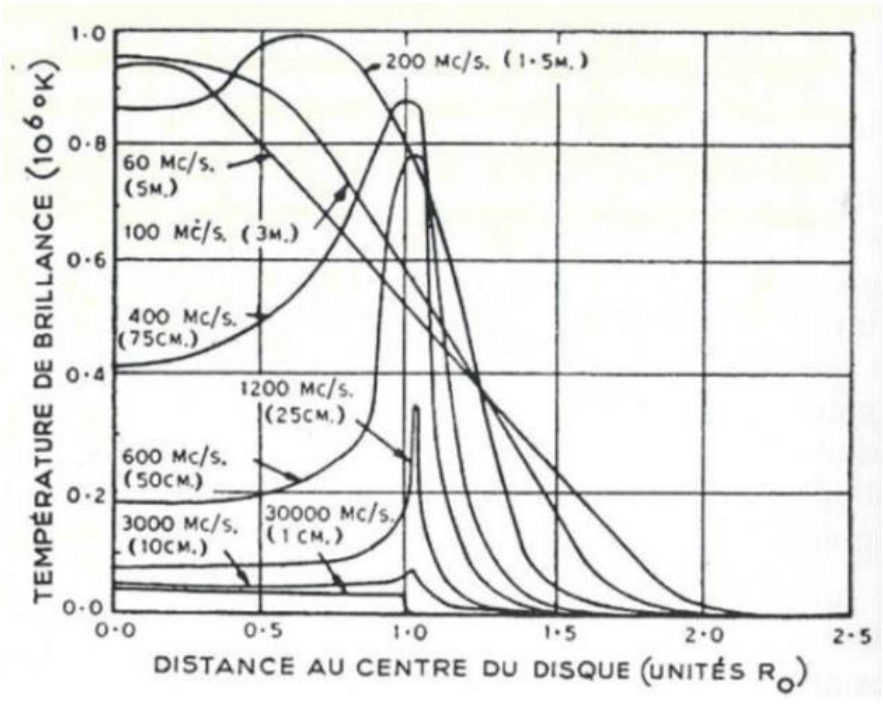

- Simulations –Model and numerical data

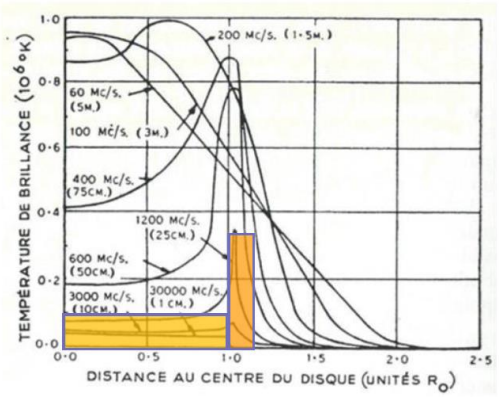

Moon radius : 0.275°
Sun corona outer radius : 0.325° (1.2 * sun rad.)
Sun corona inner radius : 0.263°

Burst n°	Radius	Azim offset	Elev offset
1	0,045	+ 0,30	-0,05
2	0,030	- 0,17	+0,21
3	0,027	- 0,31	-0,01

Eclipse magnitude is the fraction of the Sun's diameter occulted by the Moon. It is strictly a ratio of diameters and should not be confused with eclipse obscuration, which is a measure of the Sun's surface area occulted by the Moon. Eclipse magnitude may be expressed as either a percentage or a decimal fraction (e.g., 50% or 0.50). By convention, its value is given at the instant of greatest eclipse.
Eclipse obscuration is the fraction of the Sun's area occulted by the Moon. It should not be confused with eclipse magnitude, which is the fraction of the Sun's diameter occulted by the Moon. Eclipse obscuration may be expressed as either a percentage or a decimal fraction (e.g., 50% or 0.50).
http://eclipse.gsfc.nasa.gov/SEgoogle/SEgoogle2001/SE2015Mar20Tgoogle.html

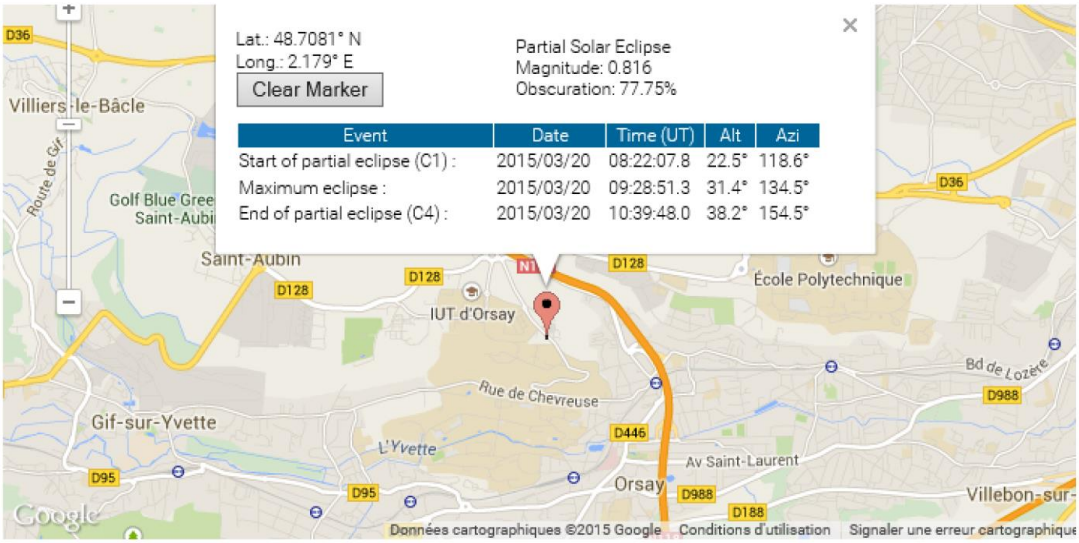

August 2015

DL0SHF

RATAN-600

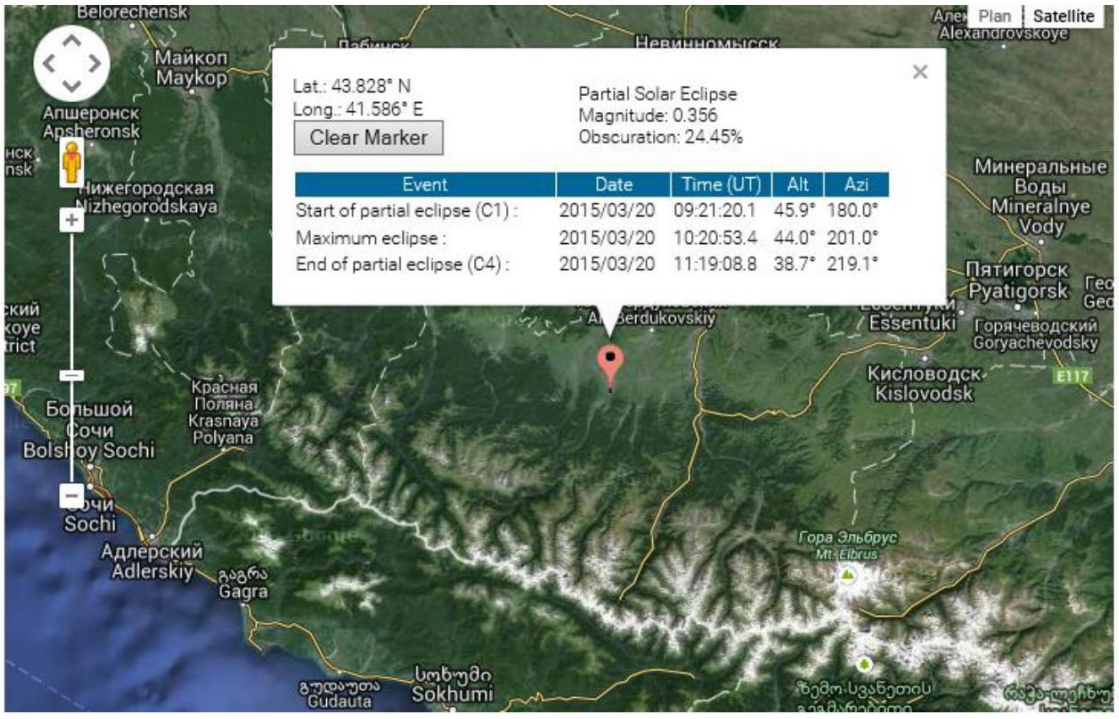

August 2015

Python programming

Using Python for real time audio FFT

By Jeff Lashley (EAARO)

Introduction

This application is intended to demonstrate ways to handle real time FFT and display it in a window. It is not intended to be a complete application to record or process the data. Clearly however it could form part of an application for SID or meteor scatter work.

It was written for Python 2.7, and requires a few packages to be installed first. It has been tested on Lubuntu Linux on an old laptop, its use on a Windows platform is untested. While most of the required packages can be installed from binary distributions on Windows the portaudio package may well require compilation from source. It is much easier to install the requirements in a Linux environment, using the easy_install or pip tools. Initial experiments with a raspberry Pi failed. This failure was probably due to the lack of conventional audio card hardware. I will further explore its functionality on the Pi in future, as well as expand its features to allow data recording and meteor detection.

Prerequisite Python packages:

- Pyqtgraph
- Pyqt4
- Numpy
- Pyaudio
- Portaudio

The code listing:

The comments in green are intended to explain the function of the lines below. Note also the line indentation is very important in Python applications.
I do find that often on first run the graph appears to freeze, but on subsequent runs it updates as normal. This may be a quirk of my hardware, the cause is unknown.

```
#!/usr/bin/python
# -*- coding: utf-8 -*-
"""
EAARO realtime FFT example
By Jeff Lashley

"""
# Import all the required packages, those highlighted in yellow are built in Python packages
from pyqtgraph.Qt import QtGui, QtCore
import numpy as np
import pyqtgraph as pg
from pyqtgraph.ptime import time
import pyaudio
import threading
```

```
import sys

# Create the main class which contains the functions
class capture:
        # init is automatically called when the class in instatiatied and sets up required
variables and interfaces
    def __init__(self):
        #setup variables relating to sound capture
        self.sampRate=48100
        self.BUFFERSIZE=2**12
        self.secToRecord=.1
        self.threadsDieNow=False
        self.newAudio=False

        #setup sound card.
        self.buffers=int(self.sampRate*self.secToRecord/self.BUFFERSIZE)
        if self.buffers==0: self.buffers=1
        self.samples=int(self.BUFFERSIZE*self.buffers)
        self.blocks=int(self.samples/self.BUFFERSIZE)
        self.secPerPoint=1.0/self.sampRate

        #create a pyaudio object
        self.p = pyaudio.PyAudio()
        #  create an input audio stream object, a 16bit one channel audio channel
        self.inStream =
self.p.open(format=pyaudio.paInt16,channels=1,rate=self.sampRate,input=Tru
e,frames_per_buffer=self.BUFFERSIZE)

        # create audio data buffers, note the audio samples are stored in a numpy (np) arrays
        self.dataBuffer=np.arange(self.BUFFERSIZE)*self.secPerPoint
        self.data=np.arange(self.blocks*self.BUFFERSIZE)*self.secPerPoint
        self.audio=np.empty((self.blocks*self.BUFFERSIZE),dtype=np.int16)

    # start recording  in a new thread
    def start(self):
        self.t = threading.Thread(target=self.record)
        self.t.start()

    # Capture sound #
        def captureAudio(self):
        #get a buffer size of audio
        audioString=self.inStream.read(self.BUFFERSIZE)
        # return the data samples as a numpy array
        return np.fromstring(audioString,dtype=np.int16)

    def record(self,forever=True):
        #record secToRecord seconds of audio.
        while True:
            if self.threadsDieNow: break
            for i in range(self.blocks):

self.audio[i*self.BUFFERSIZE:(i+1)*self.BUFFERSIZE]=self.captureAudio()
            self.newAudio=True
```

```
            if forever==False: break

    def fft(self,data=None,limit=0,logScale=False,divBy=100):
        # limit used to reduce the display bandwidth. limit 0 gives full 20kHz
        # limit 2 would give 10kHz etc
        # divby scales the y axis

        if data==None:
            data=self.audio.flatten()
        left,right=np.split(np.abs(np.fft.fft(data)),2)
        ydat=np.add(left,right[::-1])

        if logScale:
            ydat=np.multiply(20,np.log10(ydat))

        xdat=np.arange(self.BUFFERSIZE/2,dtype=float)

        # X axis scaling factor
        xdat=xdat[:int((self.BUFFERSIZE/2))]*self.sampRate/self.BUFFERSIZE

        if limit:
            # Scale X axis by:-
            i=int((self.BUFFERSIZE/2)/limit)
            ydat=ydat[:i]
            xdat=xdat[:i]*self.sampRate/self.BUFFERSIZE

        if divBy:
            ydat=ydat/float(divBy)

        return xdat,ydat

    def update(self):
        # Plot data when new buffer becomes available
        if self.newAudio==False:
            return
        xdat,ydat=self.fft()
        self.newAudio=False
        global app, curve, ptr, p
        curve.setData(xdat,ydat)
        ptr += 1
        app.processEvents()  ## force complete redraw for every plot

# Start Qt event loop unless running in interactive mode.
if __name__ == '__main__':
        # app creates the Qt GUI object
    app = QtGui.QApplication([])
    # cap in the instance of the class capture
    cap = capture()
    # p is the pyqtgraph object. Pyqtgraph is a very high performance graphing tool
    p = pg.plot()
    # setup the graph properties
    p.setWindowTitle('EAARO real-time audio FFT ')
```

```
p.setRange(QtCore.QRectF(0, 0, 20000, 150))
p.setLabel('bottom', 'Frequency', units='Hz')
p.setLabel('top', 'EAARO realtime audio FFT')
#display the plot window
curve = p.plot()
# start the audio capture and processing
cap.start()

ptr = 0
# timer is used to perform regular updates to the display (every 0.1 second)
timer = QtCore.QTimer()
timer.timeout.connect(cap.update)
timer.start(0.1)

if (sys.flags.interactive != 1) or not hasattr(QtCore, 'PYQT_VERSION'):
    QtGui.QApplication.instance().exec_()
```